When applied perturbation methods to Reynolds equation. The dimensionless time independent modified Reynolds equation can be written as

$$\frac{\partial}{\partial X}\left(\bar{\varepsilon}_U \frac{\partial P}{\partial X}\right) + \left(\frac{1}{k^2}\right)\frac{\partial}{\partial X}\left(\bar{\varepsilon}_V \frac{\partial P}{\partial Y}\right) = \Lambda\left\{cos(\psi)\frac{\partial}{\partial X}(\bar{\rho}H) + \frac{sin(\psi)}{k}\frac{\partial}{\partial Y}(\bar{\rho}H)\right\} \quad (3)$$

Where

$$\bar{\varepsilon}_U = \frac{\bar{\rho}H^3}{\bar{\mu}_U^*}, \quad \bar{\varepsilon}_V = \frac{\bar{\rho}H^3}{\bar{\mu}_V^*}, \quad \bar{\mu}_U^* = \bar{\mu}_R\left(\bar{\mu}_S^* + (n-1)\left(\bar{\mu}_S^* - \frac{\mu_\infty}{\mu_0}\right)\left(\frac{\lambda^2 K_{SH}\bar{I}_X^*}{1+\lambda^2 K_{SH}\bar{I}^*}\right)\right)$$

$$\bar{\mu}_V^* = \bar{\mu}_R\left(\bar{\mu}_S^* + (n-1)\left(\bar{\mu}_S^* - \frac{\mu_\infty}{\mu_0}\right)\left(\frac{\lambda^2 K_{SH}\bar{I}_Y^*}{1+\lambda^2 K_{SH}\bar{I}^*}\right)\right) \text{ and } \Lambda = \frac{96\mu_0 R^2 V}{P_H D_X D_Y^2}$$

Boundary conditions are

$$P(X_{inlet}) = P(X_{exit}) = (\partial P/\partial X)_{X=X_{exit}} = 0 \text{ and } P(Y_{inlet}) = P(Y_{exit}) = (\partial P/\partial y)_{Y=Y_{exit}} = 0$$

Apparent viscosity of the lubricant

The apparent viscosity in the Carreau viscosity model needs to be included the correction factor for viscosity–pressure [8]. The dimensionless apparent viscosity can be written as.

$$\bar{\mu}^* = \bar{\mu}_R\bar{\mu}_S^* \quad (4)$$

Where

$$\bar{\mu}_R = \exp\left\{\begin{matrix}(\ln(\mu_0)+9.67)\\ \times(-1+(1+5.1\times10^{-9}P_H P)^{z_1})\end{matrix}\right\} \text{ and } \bar{\mu}_S^* = \frac{\mu_\infty}{\mu_0} + \left(1-\frac{\mu_\infty}{\mu_0}\right)(1+\lambda^2 K_{SH}\bar{I}^*)^{\frac{n-1}{2}}$$

Density of the lubricant

The dimensionless density of lubricant according to Dowson and Higginson [1] obeys the following relation

$$\bar{\rho} = 1 + (0.6\times10^{-9}P_H P/\{1+1.7\times10^{-9}P_H P\}) \quad (5)$$

Film thickness

The film thickness, including the deformation of surface under line contact, is given as

$$H = H_0 + \frac{X^2}{2k\left(\frac{R_X}{R}\right)} + \frac{X^2}{\left(\frac{2}{k}\right)\left(\frac{R_X}{R}\right)} + D(X,Y) - \frac{4P_H R}{\pi E' D_X}\int_{-\infty}^{\infty}\int_{-\infty}^{\infty}\frac{P(X',Y')dX'dY'}{\sqrt{(X-X')^2+k^2(Y-Y')^2}} \quad (6)$$

Where $D(X,Y)$ is the dimensionless combined surface roughness with random roughness distribution.

Load carrying capacity

The total load carrying capacity of the lubricant is due to hydrodynamic action. The dimensionless form of load balance equation is

$$\int_{-\infty}^{\infty}\int_{-\infty}^{\infty} P(X,Y)dXdY = \frac{2\pi}{3} \quad (7)$$

Friction coefficient

The friction coefficient of surface roughness elastohydrodynamic lubrication is defined as

$$f = \sqrt{f_X^2 + f_Y^2}/w \quad (8)$$

Where

$$f_X = \frac{2\mu_0 \bar{u} R}{D_Y} \int_{X_{inlet}}^{X_{exit}} \left(\frac{\bar{\mu}^*}{H}\right)\left(\frac{\partial u^*}{\partial Z}\right)_{Z=0} dX \quad \text{and} \quad f_Y = \frac{2\mu_0 \bar{v} R}{D_X} \int_{X_{inlet}}^{X_{exit}} \left(\frac{\bar{\mu}^*}{H}\right)\left(\frac{\partial v^*}{\partial Z}\right)_{Z=0} dY$$

Simulation and Results

The material data and the properties of lubricant used in the analysis are given in Table 1 and Table 2 respectively.

Table 1 Material data of the ball and plate

Material Property	Ball	Plate
Modulus of Elasticity, GPa	200	200
Poison Ratio	0.3	0.3
Density, kg/m^3	7750	7750
Combine Amplitude Roughness, μm	0.15	

Table 2 Property of lubricant [9]

Lubricant Property	PAO-100
Inlet Density, kg/m3	834
Low Shear Strain Rate Viscosity, Pa-s	0.0698
High Shear Strain Rate Viscosity, Pa-s	0.00
Time Relaxation, s	4.657×10^{-7}
Power Law Index	0.625
Viscosity-Pressure Index	0.3917

Fig. 1, Fig.2, Fig.3 and Fig.4 show the film pressure profile and film thickness in the contact region under w=1,500 N, V=1.25 m/s and the combined surface roughness amplitude, R_{rms}=0.15 μm. For smooth surface, it can be seen that the maximum film pressure reaches its maximum at the center in the contact region, and the minimum film thickness occurs near the exit in the contact region. For rough surface, the surface roughness profile, and surface asperity have significant affected the film pressure in the contact region.

Increasing the amplitude of surface roughness, the friction coefficient increases but the minimum film thickness decreases. For smooth surface, the minimum film thickness and the friction coefficient are 0.307 μm and 0.0223 respectively. When the combined roughness is increased to 0.15 μm and 0.30 μm, respectively, the minimum film thickness decreases to 0.249 μm and 0.183 μm but the friction coefficient increases to 0.037 and 0.114respectively as shown in Fig. 5.

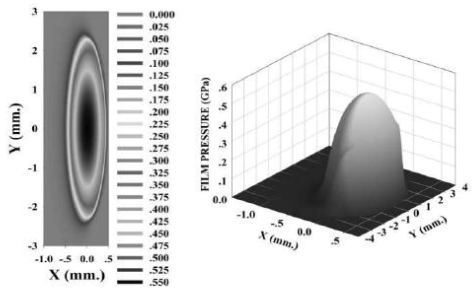

Fig 1. Film pressure profile of smooth surface

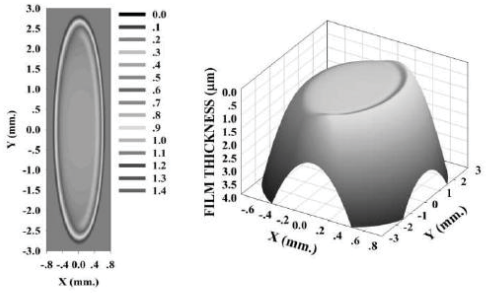

Fig 2. Film thickness profile of smooth surface

Fig. 6 shows the variation of minimum film thickness and friction coefficient for various loads. The film thickness decreases but the friction coefficient increases when the applied loads increased. For rough surface, when the applied load, w=1,500 N, the minimum film thickness and the friction coefficient are 0.299 μm and 0.037, respectively. When the applied loads increase to 2,500 N, the minimum film thickness decreases to 0.239 μm but the friction coefficient increases to 0.059.

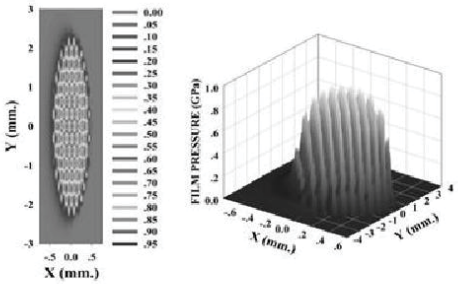

Fig 3. Film pressure profile of rough surface

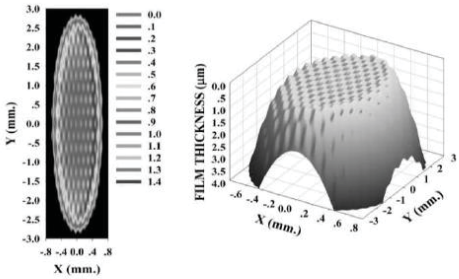

Fig 4. Film thickness profile of rough surface

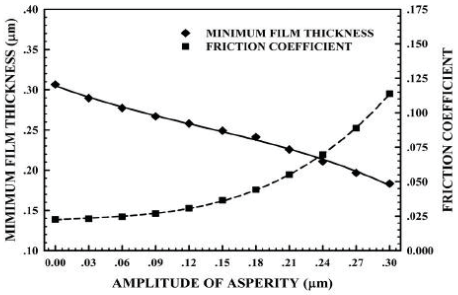

Fig 5. Minimum film thickness and friction coefficient when various amplitude of surface roughness.

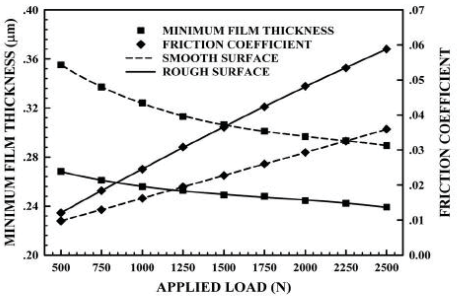

Fig 6. Minimum film thickness and friction coefficient when various applied loads.

The variation of the minimum film thickness and the friction coefficient for various average surface speeds were presented in Fig 7. The minimum film thickness increases and the friction coefficient slightly increase when surface speed increases.

Fig. 8 shows the variation of minimum film thickness and friction coefficient for varying the elliptic ratios. When elliptic ratio increases, the friction coefficient decreases but the minimum film thickness slightly increased.

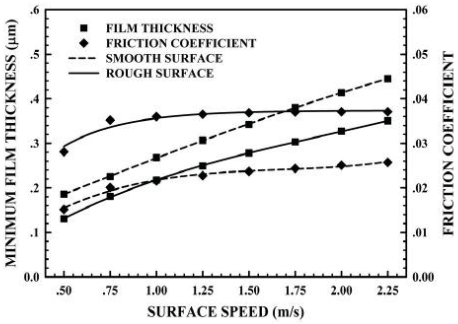

Fig 7. The minimum film thickness and friction coefficient when various surface speed

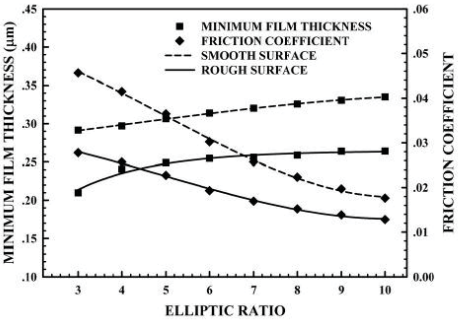

Fig 8. The minimum film thickness and friction coefficient when various elliptic ratio

Conclusion

In this research, the time independent modified Reynolds equation and elastic equation were solved to obtain minimum film thickness and friction coefficient of rough EHL in elliptical contact with non-Newtonian lubricant and can be concluded as:

1. The surface roughness has significant affect to film pressure in the contact region. The minimum film thickness decreases but friction coefficient increases when the amplitude of surface roughness increased.
2. Minimum film thickness decreases but friction coefficient increases when applied loads increases.
3. Minimum film thickness and friction coefficient both become increased as the speed increases.
4. Minimum film thickness increases but friction coefficient decreases due to the increasing of the elliptic ratio.

Acknowledgements

This research was supported by grant from Thailand Research Fund; Grant No. BRG-5180019. The additional support was received through DSI, KMITL, NSTDA and Bangkok University Thailand.

Nomenclature

$D_X/2$, $D_Y/2$	Semi-width of Hertzian's contact on x,y direction, m	R_X, R_Y	Radius of curvature on x/y direction, m
E'	Effective elastic modulus of Roller/Plate, Pa	S_X, S_Y	Slip ratio on x,y direction, m,
H	Dimensionless film thickness	V	Average surface velocity, m/s,
$\bar{I}^*$	Dimensionless second invariant of strain rate	w	Applied load ,N
$\bar{I}_X^*, \bar{I}_Y^*$	Dimensionless second invariant of strain rate on x/y direction	X, Y, Z	Dimensionless coordinate,
k	Elliptic ratio	Z_1	Viscosity-Pressure index
n	Power law index	μ	Equivalent viscosity, Pa-s
P	Dimensionless film pressure,	μ_0/μ_∞	Viscosity at low/high shear strain rate, Pa-s
P_H	Hertzian's contact pressure, Pa	ρ_0	Inlet density of lubricant ,kg/m^3
R	Radius of curvature, m	$\bar{\rho}$	Dimensionless density, $\bar{\rho} = \rho/\rho_0$
		λ	Time relaxation, s
		ψ	Angle of surface velocity, rad,

References

[1] D., Dowson and G.R., Higginson, : *Elastohydrodynamic Lubrication : The Fundamental of Roller and Gear Lubri-cation*, *Pergamon*, Oxford, (1966).

[2] C.C., Kweh, H.P., Evans, and R.W., Snidle : *Microelastohydrodyna-mic lubrication of an elliptical contact with transverse and three-dimensional roughness*, J. Tribology, Vol. 111 (1989), pp. 577-583.

[3] R.T., Lee and B. J., Hamrock : *A circular non-Newtonian fluid model: Part II - used in micro-elastohydrodynamic lubrication*, J. Tribology, Vol. 112 (1990), pp. 497-505.

[4] A.A., Lubrecht, W.E., Ten Napel and R. Bosma : *Multi-grid, an Alternative Method for Calculating Film Thickness and Pressure Profiles in EHL Line Contacts*, J. Tribology, Vol. 108 (1986), pp. 551–556.

[5] F.K., Osborn, and F., Sadeghi : *Time Dependent Line EHD Lubrication Using the Multigrid/Multilevel Technique*, J. Tribology, Vol. 114 (1992), pp. 68–74.

[6] W.Z., Wang, H., Chen, Y.Z., Hu, and H., Wang : *Effect of surface roughness parameters on mixed lubrication characteristics*, Tribology International, Vol. 39 (2006), pp. 522–527.

[7] R.I., Tanner : *Engineering Rheology*, Vol. 14–15 (1985), Clarendon Press, Oxford, pp. 359.

[8] C.J.A., Roelands : *Correlational Aspects of the Viscosity-Temperature-Pressure Relationship of Lubricating Oils*, Druk, V.R.B., Groingen, Netherland, 1969.

[9] S., Bair and F.,Qureshi : *The high pressure rheology of polymer-oil solutions*, Tribology International, Vol. 36 (2003), pp. 637-645.

Advanced Composite Materials
10.4028/www.scientific.net/AMR.482-484

Effects of Surface Roughness on Elastohydrodynamic Lubrication in Elliptical Contact with Non-Newtonian Fluids
10.4028/www.scientific.net/AMR.482-484.1057

Advanced Materials Research Vols. 482-484 (2012) pp 1426-1430
Online available since 2012/Feb/27 at www.scientific.net

doi:10.4028/www.scientific.net/AMR.482-484.1426

Effect of Solid Particle on TEHL under Line Contact with Solid-Liquid Lubricant

S. Rattapasakorn[1, a] and M. Mongkolwongrojn[2, b]

[1, 2] Department of Mechanical Engineering

King Mongkut's Institute of Technology Ladkrabang, Bangkok 10520, Thailand

[a]sountaree.t@bu.ac.th, [b]kmmongko@kmitl.ac.th

Keywords: Microfluid lubricant, TEHL, Modified Reynolds equation, Energy equation

Abstract The two infinitely long surfaces in line contact under thermoelastohydrodynamic lubrication with solid-liquid lubricants were investigated. The time-dependent modified Reynolds equation elasticity equation and the adiabatic energy equation have been formulated and solved numerically with initial conditions using multi-grid multi-level method with full approximation technique. The characteristics of the two surfaces in line contact under thermoelastohydrodynamic lubrication were presented as; film pressure, film temperature and oil film thickness profiles. The results of solid-liquid lubricants with micro-particle and nano-particle under thermal elastohydrohynamic lubrication were compared with the case of pure liquid lubricant.

Introduction

The lubricant film on the solid surfaces of the machine components operated in severe conditions become very thin. Therefore, the lubricant containing solid particles has greatly improved the lubrication characteristics in order to protect the contact surfaces. The surface temperature is significant factor for lubricating film to withstand shear stresses without being ruptured and repeated contacts for a long duration [1]. Dowson and Higginson [2] solved the numerical solution of EHL in 1959. The Newton-Raphson method was introduced to calculated EHL problem by Lee and Hamrock [3] in 1989. Jaw-Ren Lin [4] showed that couple stress fluid increase load carrying in the squeeze film when commpare with Newtonian lubricant. Mongkolwongrojn and et al [5] investigated the film temperature and film thickness of the lubricant mixed with micro size solid particles in contact region under sudden load with non-Newtonian lubricant. In 2010 W. Habchi and et al. [6] validated thermal EHL framework for the calculation of film thickness and friction coefficient in order to investigate the effects of material properties. D.X. Peng and et al. [7] showed that diamond and SiO_2 nanoparticles as additive in liquid paraffin oil have better anti-wear and anti-friction properties than that for pure paraffin oil. Murched, Leong and Yang [8] founded that the effective thermal conductivity and viscosity of nanofluids were found to significantly increase with the particle volume fraction. Rattapasakorn and Mongkolwongrojn [9] showed a behavior of thin film lubricant with focusing on temperature effect of contact surface. It is found that the film pressure increase but film thickness decrease due to the temperature in the contact regime under TEHL. Therefore, the advantages of the solid particles are to minimize the effect of temperature on thin-film lubrication and to reduce wear in the contact region.

Governing equation

The time independent dimensionless modified Reynolds equation for infinitely long line contact can be expressed as:

$$\frac{\partial}{\partial X}\left(g\frac{\partial P}{\partial X}\right) = K\left(\frac{\partial}{\partial X}(\bar{\rho}H)\right) \tag{1}$$

Where

$$K = \bar{u}\mu_0 R_x^2/b^3 P_H \,, \qquad g = \bar{\rho}H^3/\bar{\eta}$$

The Boundary conditions are

$$X = X_{in}\ , P = 0;\quad X = X_{out}\ , P = \partial P/\partial X = 0$$

Viscosity equation

The viscosity of a Newtonian lubricant depends on pressure and temperature [10]. For the viscosity of liquid-solid lubrication in this work can be written as [11], [12]

$$\bar{\mu} = \bar{\mu}_R.\bar{\mu}_s \tag{2}$$

Where

$$\bar{\mu}_R = \exp\{(\ln(\mu_0) + 9.67)(-1 + (1 + 5.1 \times 10^{-9} P_H P)^{z_2}) - \gamma T_0(\bar{\theta} - 1)\}$$

Density equation

The dimensionless density of Newtonian lubricant according to Dowson and Higginson[13] is followed as

$$\bar{\rho}_L = \left\{1 + \frac{0.6 \times 10^{-9} P_H P}{1 + 1.7 \times 10^{-9} P_H P}\right\}\left(1 - \beta T_0(\bar{\theta} - 1)\right) \tag{3}$$

Film Thickness Equation

Including the deformation of the surfaces under line contact the dimensionless film thickness equation can be written as

$$H_i = H_0 + \frac{X_i^2}{2} - \frac{\Delta X}{2\pi}\sum_{j=0}^{N} P_j\left[\left|\frac{X_{i+1} + X_i}{2} - X_j\right|\left|\frac{X_i + X_{i-1}}{2} - X_j\right|\right] \tag{4}$$

Energy Equation

The dimensionless energy equation under line contact according to Hua and Khonsari [14] can be obtained as

$$\frac{\partial^2\theta}{\partial Z^2} = K_{T1}\left[\frac{\bar{\rho}H^2}{\bar{k}_p}\right]\left[U\frac{\partial\theta}{\partial X}\right] - K_{T2}\left[\frac{\bar{\mu}}{\bar{k}_p}\right]\left[\frac{\partial U}{\partial Z}\right]^2 - K_{TB}\left[\frac{\theta H^2}{\bar{k}_p}\right]\left[U\frac{\partial P}{\partial X}\right] \tag{5}$$

Where

$$K_{T1} = \frac{\bar{u}\rho_0 C_p b^3}{k_0 R_X^2},\ K_{T2} = \frac{\mu_0\bar{u}^2}{k_0 T_0},\ K_{TB} = \frac{\beta\bar{u}b^3 P_H}{k_0 R_X^2},\ \bar{k}_p = 1 + \frac{1.73 \times 10^{-9} P_H P}{1 + 6.91 \times 10^{-9} P_H P}$$

The Boundary conditions are

$$\theta_{S1/S2} = 1 + D_{1/2}\int_{X_{in}}^{X_i}\left[\frac{\bar{k}_p}{H}\right]\left[\frac{\partial\theta}{\partial Z}\right]_{Z=0/1}\frac{dX'}{\sqrt{X_i - X'}}$$

$$D_{1/2} = \frac{k_0 R_X}{\sqrt{\pi\bar{u}\rho_{1/2}C_{p1/2}k_{1/2}b^3\left[1 \pm \frac{S_x}{2}\right]}},\ \theta_{(X=0)} = 1$$

Numerical Solution

This research is to solve the effect of particles in solid-liquid lubricant in line contact using Newton-Raphson and multi-grid multi-level method to obtain film pressure, film thickness and film temperature in the contact region. The surfaces of roller and the solid-liquid lubricant properties for the calculated are given in Table 1 and Table 2.

Table 1 Physical properties of lubricant and roller material

Property	Roller	Property	SAE-90
Elasticity modulus, GPa	205	Inlet density, kg/m^3	892.80
Density, kg/m^3	7850	Inlet viscosity, Pa-s	0.1946
Poison ratio	0.30	Viscosity-Pressure index	0.5685
Specific heat, J/(kg-K)	475	Specific heat, J/(kg-K)	1870
Thermal conductivity, W/(m-K)	50.20	Thermal conductivity, W/(m-K)	0.126

Table 2 Physical properties of Alumina [15]

Property	Alumina
Density, kg/m^3	3890
Specific heat, J/(kg-K)	729
Thermal conductivity, W/(m-K)	36
Friction Coefficient steel-alumina	0.60
Hardness, GPa	14.124

Results and Discussion

In this research, the two surfaces in line contact under thermal elastohydrodynamic lubrication with SAE-90 oil mixed with alumina particles were investigated. The applied load and mean velocity of roller are 250,000 N/m and 0.96 m/s respectively. The particle size is 2 μm in diameter and percentage of volume fraction is 0.01%. The results show that the film temperature profile and the film pressure profile are almost similar shape but the film temperature decreases rapidly at the exit in the contact region and remained stable at approximately 50 °C. Near the exit of contact region, pressure spike occurs and increases up to 0.641 GPa for film thickness and film temperature at 1.416 μm and 99.14 °C respectively.

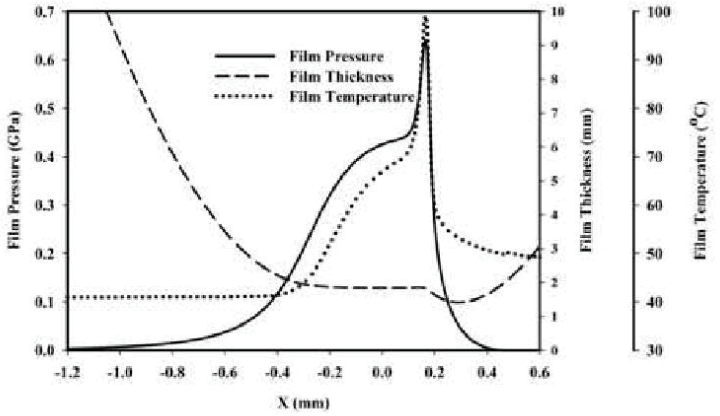

Fig.1 Film pressure, film thickness and temperature profiles for 2 μm alumina particles mixed with SAE-90.

In Figure 2, the maximum pressure of the film pressure profile is 0.635 GPa at x = 0.141 mm for SAE 90 and SAE 90 mixed with micro size particles but the maximum film pressure is only 0.599 GPa at x = 0.222 mm for SAE 90 mixed with nano size particles.

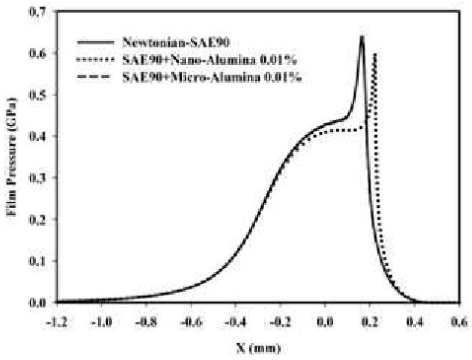

Fig.2 Pressure profiles at various lubricant.

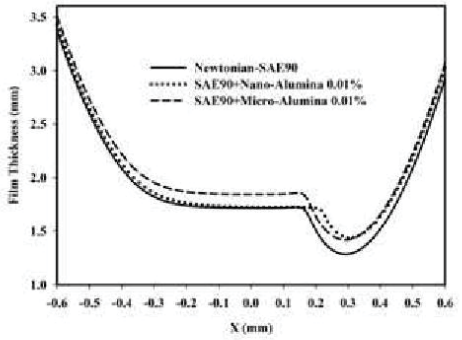

Fig.3 Film thickness profiles at various lubricant.

The minimum film thickness for SAE 90 is 1.282 μm. For SAE 90 mixed with micro size particles and SAE 90 mixed with nano size particles, the minimum film thickness are 1.416 μm and 1.437 μm respectively as shown in Figure 3. Figure 4 shows the maximum temperature for SAE 90 oil, and SAE 90 mixed with micro size particles are both equal to 100 °C. The maximum temperature is 42.05 °C for SAE 90 mixed with nano size particles.

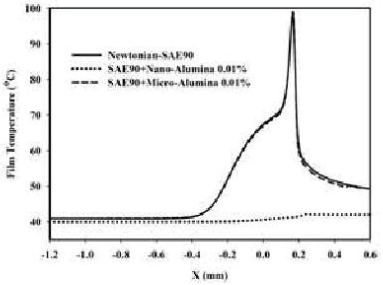

Fig.4 Film temperature profiles at various lubricant.

Conclusions

The transient thermoelastohydrodynamic lubrication characteristics of two surfaces line contact with liquid-solid non-Newtonian fluids were examined numerically. The main results presented can be summarized as:

1. For Sae 90 mixed micro size particles, The film pressure profile, film thickness profile and film temperature profile are almost identical with that for SAE 90 lubricant.
2. For Sae 90 mixed nano size particles, The film temperature decreases rapidly and the maximum temperature position shift to the exit region.

Acknowledgment

This research was supported by grant from Thailand Research Fund; Grant No. BRG-5180019. The additional support was received through DSI, KMITL, NSTDA and Bangkok University Thailand.

Nomenclature

b	Semi-width of Hertzian contact, m	μ_0	Inlet viscosity, Pa-s
H	Dimensionless film thickness	$\bar{\mu}_s$	Dimensionless viscosity of Microfluid, Pa-s
$\bar{k}_g$	Dimensionless thermal conductivity	ρ_0	Inlet density of lubricant ,kg/m^3
P_H	Hertzian's contact pressure, Pa	β	Coefficient of thermal expansively, 1/K
R_x	Radii of curvature of Roller, m	$\bar{\theta}_s$	Dimensionless surface temperature
T_0	Inlet temperature, K		
$\bar{u}$	Mean velocity of roller, m/s		
Z_1	Viscosity-Pressure index		

References

[1] Stephen M. Hsu: Nanolubrication: *Concept and Design, in Nanotribology Critical Assessment and Research Needs*, Springer, New Delhi (2006), pp. 327-346.

[2] D. Dowson and G.R. Higginson: *Numerical Solution to Elastohydrodynamic Problem*, J. Mech. Eng. Sci., vol. 1 (1959), pp. 6-15.

[3] R. Lee and B. J. Hamrock: *Squeeze and Entraining Motion in Non-conformal Line Contacts Part II: Elastohydrodynamic Lubrication*, ASME J. Tribol., vol. 111 (1989), pp. 8-16.

[4] Jaw-Ren Lin: *Squeeze film characteristics of finite journal bearings: couple stress fluid model*, Tribology International, Vol. 31 (1998), pp. 201–207.

[5] M. Mongkolwongrojn, C. Aiumpornsin and K. Thammakosol: *Theoretical Investigation in Thermoelastohydrodynamic Lubrication With Non-Newtonian Lubricants Under Sudden Load Change*, Journal of Tribology, vol. 128 (2006), pp. 771–777.

[6] W. Habchi and et al.: *Influence of pressure and temperature dependence of thermal properties of a lubricant on the behaviour of circular TEHD contacts*, Tribology International, Vol. 43 (2010), pp. 1842–1850.

[7] D. X. Peng and et al.: *Tribological properties of diamond and SiO_2 nanoparticles added in paraffin*, Tribology International, Vol. 42 (2009), pp. 911–917.

[8] S.M.S Murshed, K.C. Leong and C. Yang: *Investigations of thermal conductivity and viscosity of nanofluids*, International Journal of Thermal Science, Vol. 47 (2008), pp. 560–568.

[9] S. Rattapasakorn and M. Mongkolwongrojn: *Analysis of Two Surfaces in line contact under TEHL with Non-Newtonian Lubricants*, Applied Mechanics and Materials, Vol. 148-149 (2012), pp.736-742.

[10] Roelands, C.J.A.: *Correlational Aspects of the Viscosity-Temperature-Pressure Rela-tionship of Lubricating Oils*, Druk, V.R.B., Groingen, Netherland (1969).

[11] M. Chandrasekar, S. Suresh and A. Chandra Bose: *Experimental investigations and theoretical determination of thermal conductivity and viscosity of Al_2O_3/Water nanofluid*, Experimental Thermal and Fluid Science, Vol. 34 (2010), pp.210-216.

[12] H.G. Rylander : *A Theory of Liquid-Solid Hydrodynamic Film Lubrication*, ASLE Journal of the American Society of Lubrication Engineering (1966), pp.264-271.

[13] D. Dowson and G.R. Higginson: *Elastohydrody-namic Lubrication:The Fundamental of Roller and Gear Lubrication*, Pergamon, Oxford (1966).

[14] Hua, D. Y. and Khonsari, M. M.: *Elastohydrodynamic Lubrication by Powder Slurries, ASME J. Tribology*, Vol. 118 (1996), pp. 67-73.

[15] M. Javadi and M.Tajdari: *Experiment investigation of the friction coefficient between aluminium and steel*, Materials Science-Poland, Vol. 24 (2006), pp. 305-310.

Advanced Composite Materials
10.4028/www.scientific.net/AMR.482-484

Effect of Solid Particle on TEHL under Line Contact with Solid-Liquid Lubricant
10.4028/www.scientific.net/AMR.482-484.1426

Advanced Materials Research Vols. 452-453 (2012) pp 1291-1295
Online available since 2012/Jan/24 at www.scientific.net

doi:10.4028/www.scientific.net/AMR.452-453.1291

Transient EHL of Two Surfaces under Elliptical Contact with Non-Newtonian Lubricant

Mongkolwongrojn, Mongkol[1, a] and Panichakorn, Jesda[2, b]

[1,2]Department of Mechanical Engineering

King Mongkut's Institute of Technology Ladkrabang, Bangkok 10520, Thailand

[a]kmmongko@kmitl.ac.th, [b]s0060102@kmitl.ac.th

Keywords: Modified Reynolds equation, non-Newtonian Carreau viscosity model, elliptical contact, EHL.

Abstract. This paper presents the effects of a sudden load change and sudden speed change on the performance characteristics of two surfaces under elliptical contact with elastohydrodynamic lubrication. The non-Newtonian lubricant for the research work are modeled based on Carreau viscosity model. The time dependent modified Reynolds equation and elastic equation were formulated for compressible fluid. Perturbation method, Newton Raphson method and full adaptive multigrid method were implemented and solved to obtain the film pressure, film thickness profiles and friction coefficient in the contact regime at various applied loads and speeds. Simulation results show the friction coefficient increase significantly under sudden loads. The minimum film thickness and friction coefficient both decrease significantly as speed is decreased.

Introduction

Machine elements are often subjected to non-steady state operating conditions. For example, the cyclic variations in load are always experienced in gears and rolling element bearings, while cyclic variations in speed are often found in reciprocating seals. Transient variations in load or speed are typical examples of non-steady state operating conditions. The main characteristics of the transient variation are the sudden changes in load or speed in a relatively short period of time.

The unsteady EHL problem has historically been solved with different simplifications. The numerical solution of EHL problems was solved by Dowson and Higginson[1]. Kweh[2] and Lee[3], they started the analysis of the problem in steady state. The experimental results and the numerical solutions for the circular point contact under oscillating conditions have good qualitative agreement by Vahid[4]. Jin [5], he showed that the time period of the load impulse is important for transient condition. Lubrecht[6], he has implemented the multigrid algorithm is more efficient than the Newton-Raphson method in solving EHL with roughness effect. The multigrid technique has been developed to solve transient thermoelastohydrodynamic lubrication (TEHL) by Osborn[7].

In this paper, the transient EHL model is presented for two surfaces in elliptical contact. The combined modified Reynolds equation and elastic equations were formulated. Finite difference, multigrid multilevel method with full approximate scheme techniques and Newton's method were implemented. The characteristics of two surfaces under elastohydrodynamic lubrication with non-Newtonian lubricant for both various load change, and surface velocity change were examined.

Governing Equation

The relationship between shear stress and shear rate of non-Newtonian fluid based on Carreau viscosity model in this research work can be expressed as.

$$\tau_{xz} = \mu^*(\partial u/\partial z) \qquad \text{and} \qquad \tau_{yz} = \mu^*(\partial v/\partial z) \tag{1}$$

Applying the perturbation method, the dimensionless time dependent modified Reynolds equation can be written as

$$\frac{\partial}{\partial X}\left(\bar{\varepsilon}_U\frac{\partial P}{\partial X}\right)+\left(\frac{1}{k^2}\right)\frac{\partial}{\partial X}\left(\bar{\varepsilon}_V\frac{\partial P}{\partial Y}\right)=\Lambda\left\{C_{UT}cos(\psi)\frac{\partial}{\partial X}(\bar{\rho}H)+C_{VT}\frac{sin(\psi)}{k}\frac{\partial}{\partial Y}(\bar{\rho}H)+\frac{\partial}{\partial T}(\bar{\rho}H)\right\} \quad (2)$$

Where $C_{UT}=\bar{u}/V$, $C_{VT}=\bar{v}/V$, $\Lambda=96\mu_0R^2V/P_HD_XD_Y^2$ and $V=\sqrt{\bar{u}^2+\bar{v}^2}$ (3)

$$\bar{\varepsilon}_U=\bar{\rho}H^3/\bar{\mu}_U^*,\quad \bar{\varepsilon}_V=\frac{\bar{\rho}H^3}{\bar{\mu}_V^*},\quad \psi=tan^{-1}(\bar{v}/\bar{u}),\quad \bar{\rho}=\rho/\rho_0 \quad \text{and } k=D_Y/D_X \quad (4)$$

$$1/R=1/R_X+1/R_Y,\quad D_X/2=2(6\xi wR/\pi kE')^{1/3} \text{ and } D_Y/2=2(6k^2\xi wR/\pi E')^{1/3} \quad (5)$$

$$\bar{\mu}_U^*=\bar{\mu}_R\left(\bar{\mu}_S^*+(n-1)\left(\bar{\mu}_S^*-\frac{\mu_\infty}{\mu_0}\right)\left(\frac{\lambda^2K_{SH}\bar{I}_X^*}{1+\lambda^2K_{SH}\bar{I}^*}\right)\right),\bar{I}_X^*=\left(\frac{S_X}{H}\right)^2 \text{ and } \bar{I}_Y^*=\left(\frac{S_X}{H}\right)^2 \quad (6)$$

$$\bar{\mu}_V^*=\bar{\mu}_R\left(\bar{\mu}_S^*+(n-1)\left(\bar{\mu}_S^*-\frac{\mu_\infty}{\mu_0}\right)\left(\frac{\lambda^2K_{SH}\bar{I}_Y^*}{1+\lambda^2K_{SH}\bar{I}^*}\right)\right),K_{SH}=\left(\frac{4RV}{D_XD_Y}\right)^2 \text{ and } \bar{I}^*=\bar{I}_X^*+\bar{I}_Y^* \quad (7)$$

Boundary conditions are

$$P(X_{IN})=P(X_{OUT})=(\partial P/\partial X)_{X=X_{OUT}}=P(Y_{IN})=P(Y_{OUT})=(\partial P/\partial Y)_{Y=Y_{OUT}}=0 \quad (8)$$

The apparent viscosity equation

The apparent viscosity in the Carreau viscosity model[8] needs to be included as a correction factor for viscosity-pressure [9]. The dimensionless apparent viscosity can be written as

$$\bar{\mu}^*=\bar{\mu}_R\bar{\mu}_S^* \quad (9)$$

Where

$$\bar{\mu}_R=\exp\{(\ln(\mu_0)+9.67)(-1+(1+5.1\times10^{-9}P_HP)^{z_1})\} \quad (10)$$

$$\bar{\mu}_S^*=\mu_\infty/\mu_0+(1-\mu_\infty/\mu_0)(1+\lambda^2K_{SH}\bar{I}^*)^{\frac{n-1}{2}} \quad \text{Where} \quad P_H=6w/\pi D_X\,D_Y \quad (11)$$

The density equation

The dimensionless density of lubricant according to Dowson and Higginson[1] obeys the following relation

$$\bar{\rho}=1+0.6\times10^{-9}P_HP/(1+1.7\times10^{-9}P_HP) \quad (12)$$

The film thickness equation

The film thickness for deformation of the surfaces under elliptical contact can be written as

$$H=H_0+X^2/\left\{2k\left(\frac{R_X}{R}\right)\right\}+Y^2/\left\{\left(\frac{2}{k}\right)\left(\frac{R_X}{R}\right)\right\}-\frac{4P_HR}{\pi E'D_X}\int_{-\infty}^{\infty}\int_{-\infty}^{\infty}\frac{P(X',Y',T)dX'dY'}{\sqrt{(X-X')^2+k^2(Y-Y')^2}} \quad (13)$$

The load equation

The total load carrying capacity of the lubricant is due to hydrodynamic action. The dimensionless form of load balance equation is

$$\int_{-\infty}^{\infty}\int_{-\infty}^{\infty}P(X,Y)dXdY=\frac{2}{3}C_{WT}\pi \quad \text{Where} \quad C_{WT}=w/w_0 \quad (14)$$

The friction coefficient

The friction coefficient of surface roughness elastohydrodynamic lubrication is defined as

$$f=\sqrt{f_X^2+f_Y^2}/w \quad (15)$$

Where

$$f_X = \frac{2\mu_0 \bar{u} R}{D_Y} \int_{X_{inlet}}^{X_{exit}} \left(\frac{\bar{\mu}^*}{H}\right)\left(\frac{\partial u^*}{\partial Z}\right)_{Z=0} dX \quad \text{and} \quad f_Y = \frac{2\mu_0 \bar{v} R}{D_X} \int_{Y_{inlet}}^{Y_{exit}} \left(\frac{\bar{\mu}^*}{H}\right)\left(\frac{\partial v^*}{\partial Z}\right)_{Z=0} dY \qquad (16)$$

Computational procedure and numerical calculation

The numerical solution of the governing equations described above were solved numerically using pressure iteration. The modified Reynolds equation, elastic equation, density equation and viscosity equation under elastohydrodynamic lubrication with non-Newtonian lubricants were calculated using multigrid and Newton's method with full approximation scheme technique. The multigrid technique has been utilized to improve the convergence rate in this calculation. The convergence criteria of pressure and hydrodynamic load are adopted as follows:

$$\sum_{i=0}^{N_X}\sum_{j=0}^{N_Y} \left|P_{i,j}^{k+1} - P_{i,j}^{k}\right| \Big/ \sum_{i=0}^{N_X}\sum_{j=0}^{N_Y} P_{i,j}^{k+1} \leq 0.0001 \qquad (15)$$

$$\left|\frac{2}{3}C_{WT}\pi - \int_{X_{inlet}}^{X_{exit}}\int_{Y_{inlet}}^{Y_{exit}} P dX dY\right| \Big/ \frac{2}{3}C_{WT}\pi \leq 0.0001 \qquad (16)$$

RESULTS and DISCUSSION

The geometry and the coordinate of a ball and flat plate are defined as shown in Fig.1. The material data and the properties of lubricant used in the analysis are given in Table 1 and Table 2.

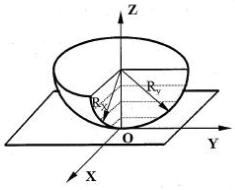

Fig. 1 Geometry and coordinate of a ball and flat plate

Table 1. Material data of the ball and plate

Material Property	Ball	Plate
Modulus of Elasticity, GPa	200	200
Poison ratio	0.3	0.3
Density, kg/m^3	7750	7756
Radius of Ball, R_X/R_Y, m	0.05/0.60	

Table 2. Property of lubricant [10]

Lubricant Property	PAO-100
Inlet Density, kg/m^3	834
Low Shear Rate Viscosity, Pa-s	0.0698
High Shear Rate Viscosity, Pa-s	0.00
Time Relaxation, s	4.657×10^{-7}
Power Law Index	0.625
Viscosity-Pressure Index	0.3917

Fig. 2, shows the contour of the film thickness in the contact region under normal load, $w_0 = 1500$ N, $V = 1.25$ m/s. For initial load, $w = 1500$ N, as shown in Fig. 2(a), the minimum film thickness is 0.306 μm at $x = 0.469$ mm and $y = 0.000$ mm. At time $t = 0.50$ ms, the dimensionless transient load, C_{WT}, is increased to 1.354 but the minimum film thickness is decreased to 0.229 μm at $x = 0.516$ mm and $y = 0.039$ mm as shown in Fig. 2(b). Fig. 2(c), shows the film thickness contour at time $t = 1.00$ ms and applied load $w = 2250$ N, the minimum film thickness increase to 0.305 μm at $x = 0.539$ mm and $y = 0.039$ mm due to the increasing of film viscosity.

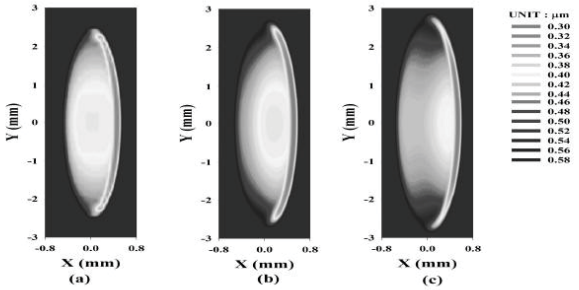

Fig. 2 Transient Film thickness contours for $w_0 = 1500$ N, $V = 1.25$ m/s and maximum $C_{WT} = 1.5$
(a) at initial condition,
(b) at time = 0.5 ms after load change and
(c) at time = 1 ms after load change

For increasing the sudden load, the minimum film thickness slightly decrease and then increase rapidly within 2 ms after that the minimum film thickness slightly decrease to the steady state condition at time approximately equal to 8.0 ms. The friction coefficient increases significantly when the load is increased. The shape of the profile on friction coefficient and applied load are very similar as shown in Fig. 3. The maximum friction coefficient are 0.0263, 0.0301 and 0.0339 for maximum sudden loads, C_{WT}, are 1.25, 1.50 and 1.75, respectively.

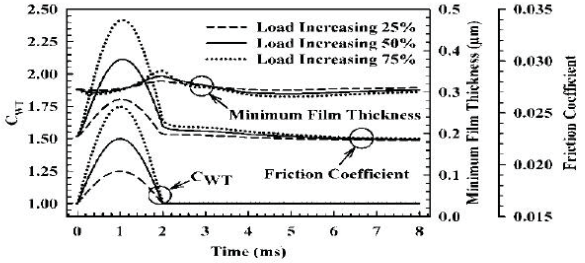

Fig.3 The dimensionless tran-sient load,C_{WT}, minimum film thickness, and friction coeffi-cient when various maximum sudden loads condition

Fig. 4, shows the film thickness contour in the contact regime under normal load, $w = 1500$ N, $V_0 = 1.25$ m/s. The minimum film thickness is 0.306 μm at $x = 0.469$ mm and $y = 0.000$ mm at the initial condition, $V = 1.25$ m/s, as shown in Fig. 4(a). At time equal to 0.50 ms, The speed is decreased to 0.808 m/s, the minimum film thickness is 0.300 μm at $x = 0.469$ mm and $y = 0.039$ mm as shown in Fig. 4(b). When time is 1.00 ms and $V = 0.625$ m/s, the minimum film thickness decrease to 0.290 μm at $x = 0.469$ mm and $y = 0.039$ mm as shown in Fig. 4(c).

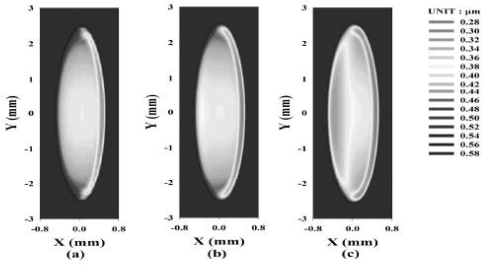

Fig. 4 Transient Film thickness contours for $w_0 = 1500$ N, $V_0 = 1.25$ m/s and minimum $C_{UT} = 0.5$
(a) at initial load and speed conditions,
(b) at time = 0.5 ms after speed change and
(c) at time = 1 ms after speed change

After reach the peak speed condition, the friction coefficient decreases speed is decreased but for time more than 1.8 ms, friction coefficient increase because of the increasing in lubricant shear strain rate. It approaches the steady state condition at time approximately equal to 7.0 ms. The minimum friction coefficients are 0.0129, 0.0146 and 0.0081 for the minimum speed, C_{UT}, are 0.75, 0.50 and 0.25, respectively. The minimum film thickness decreases when the transient sudden speed is decreased and then the minimum film thickness increases again to the steady state condition as shown in Fig. 5.

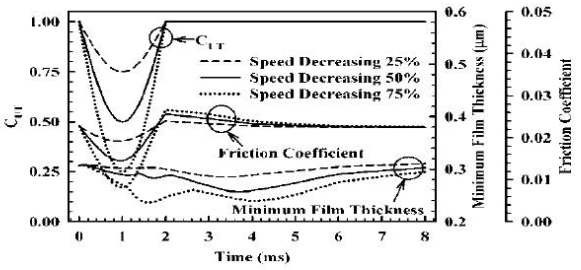

Fig. 5 The dimensionless transient speed, C_{UT}, minimum film thickness, and friction coefficient when various minimum sudden speeds condition

Conclusions

In this research, the time dependent modified Reynolds equation and elastic equation were formulated and solved numerically for two surfaces in elliptical contact with non-Newtonian lubricant under sudden change in load and speed conditions. The characteristics of two surfaces in elliptical contact under EHL were examined for isothermal condition and can be concluded as:

1. Minimum film thickness slightly decreases but friction coefficient rapidly increases when transient sudden loads increases.
2. Both minimum film thickness and friction coefficient decrease as the transient sudden speed decreases.
3. For decreasing the transient speed, C_{UT}, the film thickness at entrance contact region decreases.

Acknowledgment

This paper was supported by grant from Thailand Research Fund; Grant No. BRG-5180019. The additional funding was received through the Collage of Data Storage Innovation KMITL (DSI – KMITL) and NSTDA for research Unit on Tribology and Mechanical Engineering.

References

[1] D. Dowson, G.R. Higginson : *Elastohydrodynamic Lubrication : The Fundamental of Roller and Gear Lubrication* , Pergamon, Oxford, 1966.

[2] C.C. Kweh, H.P. Evans and R.W. Snidle : *Microelastohydrodyna-mic lubrication of an elliptical contact with transverse and three-dimensional roughness*, Trans. ASME, J. Tribology Vol. 111(1989), pp. 577-583.

[3] R.T. Lee and B.J. Hamrock : *A circular non-Newtonian fluid model: Part II - used in micro-elastohydrodynamic lubrication*, Trans. ASME, J. Tribology Vol. 112(1990), pp. 497-505.

[4] D.J. Vahid, H. Rahnejat, Z.M. Jin and D. Dowson : *Transient analysis of isothermal elastohydrodynamic circular point contacts*, Proceedings of the Institution of Mechanical Engineers, Part C: Journal of Mechanical Engineering Science Vol. 215(2001), pp. 1159-1172.

[5] Z.M. Jin, P. Yang, J. Cui and D. Dowson : *Transient elastohydrodynamic analysis of ellipti-cal contacts. Part 1: isothermal and Newtonian lubricant solution*, Proceedings of the Institution of Mechanical Engineers Part J: Journal of Engineering Tribology Vol. 218(2004), pp. 211-224.

[6] A.A. Lubrecht, W.E. Ten Napel and R. Bosma : *Multi-grid, an Alternative Method for Calculating Film Thickness and Pressure Profiles in EHL Line Contacts*, ASME, J. Tribology Vol. 108(1986), pp. 551–556.

[7] F.K. Osborn, and F. Sadeghi : *Time Dependent Line EHD Lubrication Using the Multigrid/Multilevel Technique*, ASME, J. Tribology Vol. 114(1992), pp. 68–74.

[8] R.I. Tanner : *Engineering Rheology*, Clarendon Press, Oxford, , Vol. 14–15 (1985), pp. 359.

[9] C.J.A. Roelands : *Correlational Aspects of the Viscosity-Temperature-Pressure Relationship of Lubricating Oils*, Druk, V.R.B., Groingen, Netherland, 1969.

[10] S. Bair and F. Qureshi : *The high pressure rheology of polymer-oil solutions*, Tribology International Vol. 36(2003), pp. 637-645.

Management, Manufacturing and Materials Engineering
10.4028/www.scientific.net/AMR.452-453

Transient EHL of Two Surfaces under Elliptical Contact with Non-Newtonian Lubricant
10.4028/www.scientific.net/AMR.452-453.1291

Advanced Materials Research Vols. 452-453 (2012) pp 1262-1266
Online available since 2012/Jan/24 at www.scientific.net

doi:10.4028/www.scientific.net/AMR.452-453.1262

Influence of Speed-up and Speed-down on Internal Stresses of Wound Rolls in Web handling Process

Mongkol Mongkolwongrojn[1, a] and Puttha Jeenkour [2,b]

[1,2] Mechnical Engineering, Faculty of Engineering, King Mongkut's Institute of Technology Ladkrabang (KMITL), Bangkok, Thailand 10520

[a] kmmongko@kmitl.ac.th, [b] s9060105@kmitl.ac.th

Keywords: Internal stresses, Wound roll, Speed-up, Speed-down, Web handling system, Wrinkle and Slippage

Abstract. In web winding process, the effects of speed-up and speed-down on internal stresses of wound roll have been investigated. The air-entrainment can be obtained theoretically using the modified nonlinear Hakiel model. In this research work, air-entrainment model established by Hamrock and Dowson was applied to estimate the initial air film layers into a wound roll in the winding system with a nip-roller. Moreover, the characteristics of a wound roll were examined under varying tension and varying speed conditions. The numerical results showed the radial stress, tangential stress, and friction force distributions at central inside a wound roll under the condition for a wound roll without wrinkle and slippage phenomena.

Introduction

The web handling systems are the important part of thin film production processes such as optical film, paper sheet, printed electronic film and so on which operates under using continually transported by a roll-to-roll conveyance system. Each process in web handling can be mainly shown in Fig. 1 which consists of costing, stretching, and winding. The final process of web handlings are well known and called the winding systems. The winding processes have been used for storage thin film web as multiple layers which normally called a wound roll. According to the prediction of IDTechEx report in 2009[1], the market for potentially printed electronics, including organics, inorganic and composites, will go up from $1.92 billion in 2009 to $57.16 billion in 2019. Therefore, in order to support the increasing of demand for the future, the web handing technology should be improved as soon as possible for saving energy, increasing the production efficiency, and so on. According to the history research work in flexible web technology can be found in references [2-7]. However, the previous works did not consider the effect of speed-up and speed-down in web handling process so the aim of this paper is to investigate the effect of time delay on a speed-up and a speed-down in condition that prevented a wound roll from wrinkle and slippage phenomena.

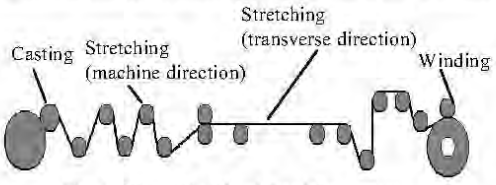

Fig. 1 Schematic of web handling process

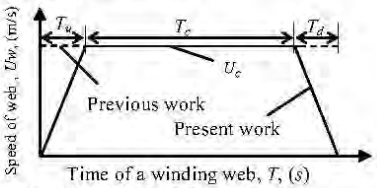

Fig. 2 Profile of winding velocity

Speed-up and speed-down delay in winding system

The speed of web through winding both previous work and present work was shown in Fig.2. The dash line is the speed of web that used in previous works, and the solid line is the speed of web including the effect of a speed-up delay, T_u, and a speed-down delay, T_d, that considered in this paper. The speed-up delay occurs in web handling processes at the beginning of operation namely when machine operates, the speed of web will increase from non-moving status to the controlled speed or

constant speed status, U_c, so this period is called a speed-up delay. In the same way, the speed-down delay occurs in web handling processes near the end of operation namely the speed of web will decrease from constant speed to non-moving condition so this period is called a speed-down delay. The mathematical model for winding speed of web through winding operation as shown in Fig. 2 can be divided to three regions and can be expressed as

$$U_{w,i}=(U_c/T_u)T_i \text{ (for } 0\le T_i< T_u);\ U_{w,i}=U_c \text{ (for } T_u\le T_i\le T_u+T_c);\ U_{w,i}=(U_c/T_d)(T_i-T_u-T_c) \text{ (for } T_i>T_u+T_c) \quad (1)$$

For the length of web that has been already reeled as a wound roll, we can evaluated by using integer of Eq. 1 so the relationship between the length of web reeled, time and the radius of a wound roll during winding can expressed as:

$$L_i=\int_{T=0}^{T=T_i} U_w dT=\sum_{i=1}^{n} 2\pi r_i \quad (2)$$

Where L_i is the length of web reeled, T_i is time, r_i is the radius of a wound roll, and the subscript of i indicate the current of web layer.

Internal stresses of a wound roll with air-entrainment

The characteristics of wound rolls can be explained with the internal stresses that consist of at least two directions as shown in Fig. 3. The radial stress is defined as σ_r and the tangential stress is defined as σ_t. By using non-linear Hakiel model including the effect of air-film layers in-roll can be expressed in Eq. 3 [6], the incremental radial stress in each layers during winding can be evaluated. According to the effect of air-film layers in-roll can be explained by the equivalent Young's modulus in radial and tangential direction (E_{req} , E_{teq}) as shown in Eq. 4 respectively.

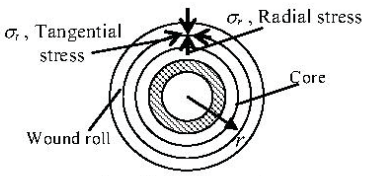

Fig. 3 Typical of internal stresses

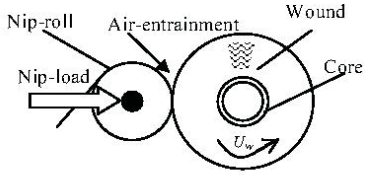

Fig. 4 Diagram of the simplest winding with nip-roll

$$r^2\left(\partial^2\Delta\sigma_r/\partial r^2\right)+(3-\upsilon)r\left(\partial\Delta\sigma_r/\partial r\right)+\left(1-E_{teq}/E_{req}\right)\Delta\sigma_r=0 \quad (3)$$

$$E_{teq}=\left(t_w/(t_w+h)\right)E_t\ ,\quad E_{req}=(t_w+h)/\left(t_w/E_r+h/E_{ra}\right)\ , \quad (4)$$

Where Young's modulus of air layer inside a wound roll with nip-load can be given as follows.

$$E_{ra}=\left(|\sigma_r|+p_a\right)^2/\left(\left(T_w|_{r_{out}}+\mu_k Nip/W\right)/r_{out}+p_a\right) \quad (5)$$

The simple winding process with nip-roll is presented in Fig. 4. Where W is the web width, t_w is the web thickness, T_w is a web tension, E_r is the radial Young's modulus, E_t is the tangential Young's modulus, υ is a Poisson's ratio of wound roll, h is the air film layer that estimated by Hamrock et al. [7] in case of the winding system with nip-roller, p_a is the ambient pressure, R_q is the equivalent RMS roughness of web, μ_s is static friction coefficient and μ_k is defined as a kinetic friction coefficient that can be estimated by Hashimoto's formulation below [8].

$$\mu_k=\mu_s \quad for\ h<R_q;\ \ \mu_k=(\mu_s/2)(3-h/R_q) \quad for\ R_q\le h\le 3R_q;\ \ \mu_k=0 \quad for\ h>3R_q \quad (6)$$

Therefore, radial stress at the ith layer of a wound roll can be evaluated by summing all increment radial stresses in each layer from the i+1 layer up to the nth layer (final layer of winding) as follows

$$\sigma_{ri} = \sum_{j=i+1}^{n} \Delta\sigma_{ri,j} \tag{7}$$

By using the force equilibrium in polar coordinate, the relationship between radial stress and tangential stress can be formulated as:

$$\sigma_t = r\left(\partial\sigma_r / \partial r\right) + \sigma_r \tag{8}$$

For friction force inside a wound roll, F_i can be written as.

$$F_i = 2\pi\, r_i \mu_{k,i} \left|\sigma_{r,i}\right| W \tag{9}$$

Wrinkle and slippage phenomena of wound rolls

Since unsuitable internal stresses of wound rolls, the wrinkle and the slippage phenomena can occur in wound rolls namely small radial stress or more air-entrainment lead to low friction force in-roll and slippage phenomenon, and the negative tangential stress in-roll (compressive stress) lead to the wrinkle phenomenon. In order to prevent problems as already mentioned, the tangential stress and friction force in-roll should be expressed as

$$\sigma_{t,i} > 0 \quad ; \; F_i > F_{ref}, \text{ for } (1.0<\text{r/rc}<2.1 \tag{10}$$

Where F_{ref} is the critical friction force that web layers in roll performs as slipping each other. According to this value for a PET wound roll, we refer to the empirical proposed by Hashimoto [8] and it is 50 gravity force.

Numerical analysis

The governing equation in Eq. 3 is discretized to N number of locations along the roll radii by using the finite different method. Once the derivatives are replaced with central difference approximations, the governing equation can be rewritten as

$$\left(r^2/\Delta r^2 - 3r/2\Delta r\right)\Delta\sigma_r(i-1) + \left(-2r^2/\Delta r^2 + 1 - E_{teq}/E_{req}\right)\Delta\sigma_r(i) + \left(r^2/\Delta r^2 + 3r/2\Delta r\right)\Delta\sigma_r(i+1) = 0 \tag{11}$$

Considering nip-induced tension, the boundary conditions at outermost and innermost of the roll can be expressed as:

$$\Delta\sigma_{r_{out}} = -\left(T_w\big|_{r_{out}} + \mu_k Nip / W\right) / r_{out} \quad ; \quad \left(d\Delta\sigma_r / dr\right)\big|_{r=r_{in}} = \left(\left(E_{teq}/E_c\right) - 1 + \nu\right)\left(\Delta\sigma_r\big|_{r=r_{in}} / r_{in}\right) \tag{12}$$

The incremental radial stress can be solved by written these equations in matrix form yields a tri-diagonal system as shown below.

$$[A]\{\Delta\sigma_r\} = [0] \tag{13}$$

The system of equation can be solved efficiently by a Gaussian elimination routine consisting of (N-1) forward and (N-1) backward substitutions.

Numerical results and discussions

In this section, the numerical results were obtained from the physical properties of materials as shown in Table 1. The web is a PET film (Polyethylene terephthalate), the core material is the wood, and the nip-roll is rubber. The results such as radial stress, tangential stress, and friction force in-roll were calculated under the beginning of winding tension is 150 N/m (T_s), the taper winding tension, the nip-load of 50 N, and the winding velocity at control point is 0.5 m/s. The formulation that explained taper winding tension can be found in Eq. (14). Where ϕ is defined as taper ratio. For this paper, winding tensions through radial position of a wound roll in the reel process such as constant tension (ϕ

=0), and taper winding tension (ϕ=0.4) are shown in Fig. 5. Figure 6 showed winding velocities through operating of reel process that consists of a constant winding velocity, and a winding velocity with a speed-up and a speed-down. Speed-up begin from *r/rc*=1.0 to *r/rc*= 1.1 or accord with 130 second (T_u =130 s) and speed-down begin from *r/rc*=1.65 to *r/rc*= 2.2 or accord with 1,328 second (T_d =1,328 s).

$$T_w = T_s - \phi(r - r_c) \tag{14}$$

Table 1. Material properties

Parameter	Value
Equivalent RMS roughness, R_q	0.066 (μm)
Web thickness, t_w	50 (μm)
Web width, W	0.28 (m)
Static friction coefficient, μ_s	0.3
Tangential Young's modulus of wound roll, E_t	4.3205 (GPa)
Radial Young's modulus of wound roll, E_r	$E_r = a\lvert\sigma_r\rvert^b$ (Pa) a = 4.09E4, b=0.65
Young's modulus of core , E_c	1.3 (GPa)
Winding core radius, r_c	0.05 (m)
Young's modulus of nip-roll, E_{nip}	0.027 (GPa)
Poisson's ratio of wound roll, υ	0.3

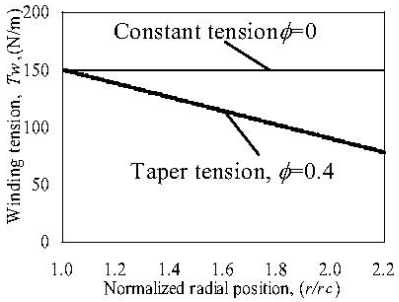

Figure 5 Winding tension

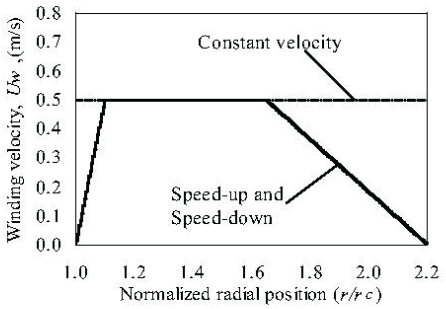

Fig. 6 Winding velocity

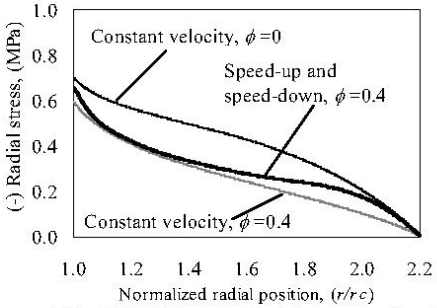

Fig. 7 Radial stress inside a wound roll

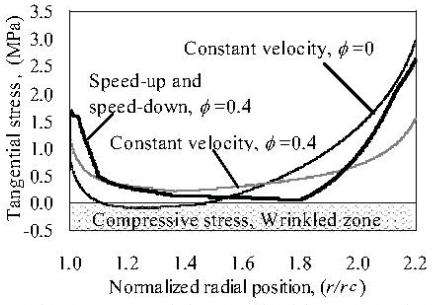

Fig. 8 Tangential stress inside a wound roll

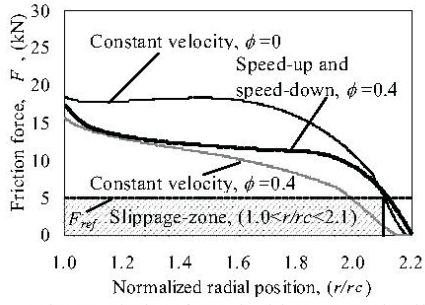

Fig. 9 Friction force inside a wound roll

Figures 7 to 9 showed the characteristics of a wound roll such as radial stress, tangential stress, and friction force in-roll under the winding conditions as mention above. The results showed that under a constant winding velocity, and a constant winding tension (ϕ=0) the radial stress in-roll become the highest value as shown in Fig. 7 and result in high friction force in-roll that become higher than the

critical friction through r/rc =1.0 to r/rc = 2.1. Therefore, a wound roll becomes no-slippage phenomenon as shown in Fig. 9. However, the tangential stress in-roll under this condition becomes negative value or compressive stress and wrinkle phenomenon occurs in a wound roll as shown in Fig. 8.

For a wound roll under a constant winding velocity, and a taper winding tension (ϕ =0.4), this condition can prevent the wrinkle phenomenon due to positive tangential stress as shown in Fig. 8. However, the radial stress in-roll becomes the lowest value and lead to low friction force that is lower than that the critical friction force from r/rc =2.0 to r/rc = 2.1 result in slippage phenomenon for theses radial positions as shown in Fig. 9.

For a wound roll under a winding velocity with a speed-up and a speed-down, and a taper winding tension (ϕ=0.4), a wound roll can be prevented from both of the wrinkle and the slippage phenomena due to through radial positions the tangential stress without negative value, and friction force in-roll from r/rc =1.0 to r/rc = 2.1 become higher than that the critical friction force as shown in Figs. 8 and 9 respectively.

Conclusions

In this paper, the winding conditions such as a constant winding velocity, a winding velocity with the effect of a speed-up and a speed-down, a constant winding tension, and a taper winding tension were theoretically investigated. The main conclusions can be summarized as follow:

1) The radial stress in-roll become significantly large in case of operating under a constant winding tension and can lead to wrinkle phenomenon.
2) The friction force in-roll become too small in the case of operating under a taper winding tension and lead to slippage phenomenon.
3) By using speed-down delay with taper winding tension, both wrinkle and slippage phenomena can be prevented efficiently and energy can be saved.

Acknowledgement

Financial support from The Royal Golden Jubilee Ph.D. Program (RGJ) for this research is greatly acknowledged. The additional funding was received through Thailand Research Fund; Grant No. BRG-5180019.

References

[1] D. Raghu and H. Peter: *Printed, Organic & Flexible Electronics Forecasts, Players & Opportunities 2009-2029*, IDTechEX, (2009).

[2] S. Fuchigami: *Challenges and Opportunities in Flat Panel Industry*, Proceedings of the Eighth International Conference on Web Handling, (2005), p.183.

[3] M.G. Catlow and G.W. Walls: *A Stability of Stress Distribution in Pirns*, Journal of Textile Institute, (1962), p.410.

[4] J.D. Pfeiffer: Tappi Journal, Vol.49 (1966), p.342.

[5] H.P. Yogoda: Mechanical Research Communications, Vol.7 (1980), p.103.

[6] Z. Hakiel: *Nonlinear Model for Wound roll Stresses*, Tappi Journal, Vol.70 (1997), p.113.

[7] B.J. Hamrock and D. Dowson: ASME J. Lubrication Technology, Vol.100 (1978), p.236.

[8] H. Hashimoto, P. Jeenkour,and M. Mongkolwongrojn: Journal of Advanced Mechanical Design, System, and Manufacturing, Vol.4 (2010), p.241.

Management, Manufacturing and Materials Engineering
10.4028/www.scientific.net/AMR.452-453

Influence of Speed-up and Speed-down on Internal Stresses of Wound Rolls in Web Handling Process
10.4028/www.scientific.net/AMR.452-453.1262

Applied Mechanics and Materials Vols. 148-149 (2012) pp 778-784
Online available since 2011/Dec/22 at www.scientific.net

doi:10.4028/www.scientific.net/AMM.148-149.778

Effect of Liquid-Solid Lubricant on Mixed Lubrication in Line Contact

Rattapasakorn Sountaree [1, a] Panichakorn Jesda [2, b]
and Mongkolwongrojn Mongkol [3, c]

[1,2,3] Department of Mechanical Engineering
King Mongkut's Institute of Technology Ladkrabang, Bangkok 10520, Thailand
[a]sountaree.t@bu.ac.th, [b]s0060102@kmitl.ac.th, [c]kmmongko@kmitl.ac.th

Keywords: Surface Roughness, Mixed Lubrication, Liquid-Solid Lubricant,

Abstract. This paper presents the performance characteristics of two surfaces in line contact under isothermal mixed lubrication with non-Newtonian liquid–solid lubricant base on Power law viscosity model. The time dependent Reynolds equation, elastic equation and viscosity equation were formulated for compressible fluid. Newton-Raphson method and multigrid technique were implemented to obtain film thickness profiles, friction coefficient and load carrying in the contact region at various roughness amplitudes, applied loads, speeds and the concentration of solid lubricant. The simulation results showed that roughness amplitude has a significant effect on the film pressure, film thickness and surface contact pressure in the contact region. The film thickness decrease but friction coefficient and asperities load rapidly increases when surface roughness amplitude increases or surface speed decreases. When the concentration of solid lubricant increased, friction coefficient and asperities load decrease but traction and film thickness increase.

Introduction

Modern engineering components are operating in the mixed lubrication regime, where the lubricant film separating the contacting surfaces is thinner than the height of their combined undeformed roughness. The lubricant in running machines has been contaminated by many solid particles. These particles may come from rust, wear debris, dust, and sometimes solid additives.

The liquid-solid mixed lubrication problem has historically been solved with different simplifications. The numerical solution of elastohydrodynamic lubrication (EHL) problems was solved by Dowson and Higginson[1]. In 1990, Khonsari, Wang, and Qi[2] formulated Reynolds and energy equations for non-Newtonian liquid-solid lubricants in line contact. The solid lubricant had significant effects in raising the film thickness, load capacity, temperature, and friction coefficient in the full EHL regime. Sayles [3] came to the conclusion that the particles lager than oil film thickness and softer than the interacting surfaces would also hurt the surface, and reduce the life of the tribopair. Yousif [4], Hisakado [5] obtained improved lubrication characteristics by mixing soft MoS2 and graphite particles with pure oil. Lubrecht, Ten Napel, and Bosma[6], showed that the multigrid algorithm is more efficient than the Newton-Raphson method in solving EHL with roughness effect. The multigrid technique has been developed to solve transient thermo-elastohydrodynamic lubrication TEHL by Osborn and Sadeghi [7]. Ai and Cheng [8] presented the formulation of the transient rough EHL problem using a multigrid technique. The results showed that surface roughness induced transient affects significantly the pressure distribution in line contact. Mongkolwongrojn[9] showed that the non-Newtonian lubricant has affects significantly to the film temperature and film thickness of lubricant in contact region under sudden load. Wang[10] presented to generate non-Gaussian surfaces with specified standard deviation of mixed lubrication.

In this paper, a mixed liquid–solid lubrication model is presented which combined Reynolds equation, the load carrying equations of the spherical particles, and Hertzian contact equation of the asperities. Finite difference, multigrid multilevel method with full approximate scheme techniques and Newton's method were implemented to calculate the mixed lubrication with non-Newtonian

under surface asperity, applied load, surface velocity and powder concentration change. To determine minimum film thickness, friction coefficient and asperity capacity at different contact points along the line of action.

Governing equation

The relationship between shear stress and shear rate of non-Newtonian lubricant in this work using a power-law viscosity model can be expressed as.

$$\tau_{xz} = \mu^*(\partial u/\partial z) \qquad and \qquad \tau_{yz} = \mu^*(\partial v/\partial z) \tag{1}$$

Where the equivalent viscosity

$$\mu^* = m_0[(\partial u/\partial z)^2 + (\partial v/\partial z)^2]^{(n-1)/2} \tag{2}$$

The dimensionless time independent modified Reynolds equation can be written as:

$$\frac{\partial}{\partial X}\left(g\frac{\partial P}{\partial X}\right) = K\left\{\frac{\partial}{\partial X}(\bar{\rho}H) + \left(\frac{S_X}{2}\right)\frac{\partial}{\partial X}\left(\bar{\rho}H\left(1-2\frac{\bar{\mu}_{s0}}{\bar{\mu}_{s1}}\right)\right)\right\} \tag{3}$$

Where

$$K = u_0\mu_0R^2/b^3P_H\ , \qquad g = \bar{\rho}H^3(1/\bar{\mu}_{s2} - \bar{\mu}_{s0}/\bar{\mu}_{s1})\ , \qquad 1/\bar{\mu}_{s1} = \int_0^1 (Z^i/\bar{\mu}^*)dZ$$

Boundary conditions are

$$X = X_{inlet}\ , P = 0 \ ;\ X = X_{exit}\ , P = \partial P/\partial X = 0$$

The apparent viscosity equation

The effect of particles on viscosity can be expressed by Einstein equation. The apparent viscosity in the power-law model needs to be included as a correction factor for viscosity-pressure [11] and the correction factor for solid particles in the lubricants according to Rylander[12]. The dimensionless apparent viscosity can be written as

$$\bar{\mu}^* = \bar{\mu}_R\bar{\mu}_S^* \tag{4}$$

Where

$$\bar{\mu}_R = \left(1 + \frac{2.5\lambda\rho_0}{\lambda\rho_0 + (1-\lambda)\rho_p}\right)\exp[(\ln(\mu_0) + 9.67)(-1 + (1 + 5.1\times10^{-9}P_HP)^{z_2})] \tag{5}$$

$$\bar{\mu}_S^* = \frac{m_0}{\mu_0}\left|\frac{u_0R_0}{b^2}\right|^{n-1}\left|\frac{1}{H}\frac{\partial u^*}{\partial Z}\right|^{n-1} \tag{6}$$

The density equation

The dimensionless density of liquid–solid lubricant according to Dowson and Higginson[1] obeys the following relation

$$\bar{\rho} = (1 + 0.6\times10^{-9}P_HP/(1 + 1.7\times10^{-9}P_HP))/\{1 - \lambda(1 - \rho_0/\rho_p)\} \tag{7}$$

Load-carrying capacity

In the mix lubrication region, the total load (W_T) carrying capacity of tribopair consists of three parts: particles capacity W_P, asperity capacity W_A and fluid capacity W_F where

$$W_T = W_F + W_P + W_A \tag{8}$$

Classically, the load supported by fluid is

$$W_F = \int_{x_{inlet}}^{x_{exit}} p(x)dx \tag{9}$$

Consider a spherically shaped of particle in the contact region under the action of normal load, the particle may undergo elastic or plastic deformation. For a particle that deforms plastically when the mean contact pressure reaches the hardness of particle, H_a, the load carried by a plastically deformed particle can be written as

$$w_{i,pl} = (9/6)\pi^3 H_a^3 (d_p/E_{ps}) + p(x) v_p A_{i,pl} \quad (10)$$

The equivalent elastic modulus of the particle and the contact surface is

$$2/E_{ps} = (1 - v_p^2)/E_p + (1 - v_s^2)/E_s \quad (11)$$

Where $A_{i,pl}$ is the contact area of an individual particle due to plastic deformation. Equations give the load carrying capacity of a single particle due to elastic and plastic deformation. Therefore, the load carrying capacity for all particles is

$$W_p = \sum_{1}^{N_X} \sum_{1}^{N_Z} w_{i,pl} \quad (12)$$

Where N_X and N_Z are numbers of particles that come in contact with the surface in x- and z-directions. The number of particles can be calculated as:

$$N_j = l_j \sqrt{\frac{V_f}{l_x l_z} \frac{6\lambda}{\pi d_p^3} \frac{\rho_0/\rho_p}{[1 - \lambda(1 - \rho_0/\rho_p)]}} \quad (13)$$

Where λ is the concentration of particles by weight, V_f is the volume of the solid-liquid lubricant within the contact region and l_j is the effective length along which the particles deform.

According to the theory of Greenwood and Tripp [13], the load capacity of asperities is

$$W_a = \frac{2}{3} n\beta\sigma_s \sqrt{\sigma_s/\beta}\, E' A_{nom} F_{\frac{3}{2}}(h(x)/\sigma_s) \quad (14)$$

The friction coefficient

The total friction force is composed of three parts: asperity friction force, particle friction force and fluid friction force. Then

$$f = \left(\int_{X_{inlet}}^{X_{exit}} \mu^* \left(\frac{\partial u}{\partial z} \right)_{z=0} dx + f_p W_p + f_a W_a \right) / W_T \quad (15)$$

Computational procedure and numerical

The time-independent Reynolds equation, film thickness and load balance of the two surfaces in line contact with non-Newtonian liquid-solid lubricants are simultaneously solved using multigrid multilevel and Newton-Raphson techniques to obtain solution with fast convergence. The convergence criteria of pressure and hydrodynamic load are adopted as follows:

$$\sum_{i=0}^{N} |P_i^{k+1} - P_i^k| \Big/ \sum_{i=0}^{N} P_i^{k+1} \le 0.0001 \quad \text{and} \quad |W_T - W_F - W_p - W_a| \le 0.0001 \quad (16)$$

During each time interval, the modified Reynolds equation and elasticity equation are calculated using boundary conditions and initial conditions to obtain pressure and film thickness distributions. In this problem, the boundary condition X_{inlet} and X_{exit} can be obtained as $X_{inlet} = -6.0$ and $X_{exit} = +2.0$.

Results and Discussion

The roller data, properties of liquid lubricant and the properties of solid lubricant used in the analysis are given in Table 1 and Table 2.

Table 1 Physical properties of lubricant and roller material

Equivalent radius, m	0.05
Equivalent modulus of elastic of rolling/sliding, GPa	225
Poisson ratio of rolling/sliding	0.3
Inlet temperature of lubricant, K	303.15
Ambient density of the lubricant, kg/m^3	892.80
Ambient viscosity of the lubricant, $Pa \cdot s$	0.114
Viscosity-Pressure index (Z_1)	0.4706
Power law index (n)	0.975

Table 2 Physical properties of solid lubricants

Brinell hardness, GPa	3.139
Modulus of elasticity, GPa	34
Poisson ratio	0.13
Density, kg/m^3	4800
Friction coefficient	0.1
Particle diameter, μm	2

Fig. 1 shows the fluid film pressure profile, film thickness and asperity contact pressure in the contact region under applied load 300 kN/m, rolling speed = 1.25 m/s, the combined surface roughness amplitude, $R_{rms} = 0.35$ μm and the deviation of the asperity height, $\sigma_s = 0.18$ μm. When average film thickness is bigger than combine surface roughness amplitude, the effects of asperities is so small that it can be ignored. But when the film thickness is relatively thin, the errors result from smooth surface is quite obvious.

The variation of the lubricant film thickness, the friction coefficient and asperity capacity for various amplitude of surface roughness, R_{rms} were presented in Fig 2. The friction coefficient and asperity capacity increased but the lubricant film thickness decreased when amplitude of surface roughness, R_{rms} was increase. For the combined roughness, $R_{rms} = 0.35$ μm, the minimum film thickness, the friction coefficient and asperity capacity are 0.284 μm., 0.124 and 15.02%, respectively. When the combined roughness is increased to 0.40 μm, the friction coefficient and asperity capacity are also increased to 0.196 and 32.29%, respectively but the minimum film thickness is decreased to 0.268 μm.

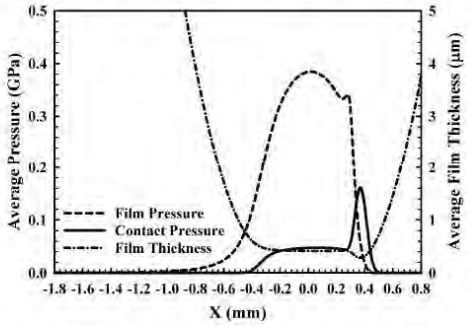

Fig.1 The fluid film pressure profile, film thickness and asperity contact pressure under applied load 300 kN/m, rolling speed = 1.25 m/s, both surface roughness amplitude, $R_{rms} = 0.35$ μm, and devia-tion of the asperity height, $\sigma_s = 0.18$ μm

For increasing the applied loads under rolling speed at 1.25 m/s, both surface roughness amplitude, $R_{rms} = 0.35$ μm, and the deviation of the asperity height, $\sigma_s = 0.18$ μm., the friction coefficient rapidly increase but the minimum film thickness is slightly decreased due to the increasing of apparent viscosity. Then, the asperity capacity is slightly increase as shown in Fig. 3. For the applied load 450 kN/m, the minimum film thickness, the friction coefficient and asperity capacity are 0.251 μm., 0.252 and 17.68% respectively.

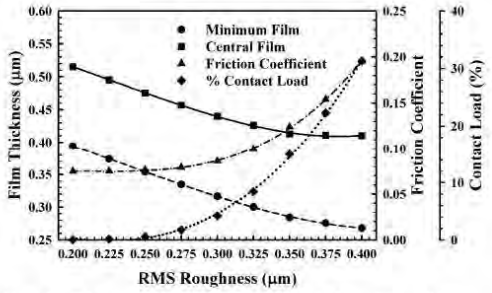

Fig.2 The variation of the lubricant film thickness, the friction coefficient and asperity capacity when various amplitude of surface roughness under applied load 300 kN/m and rolling speed = 1.25 m/s.

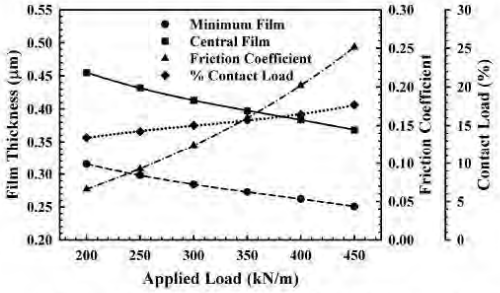

Fig.3 The variation of the lubricant film thickness, the friction coefficient and asperity capacity when various applied loads

Fig. 4 show the minimum film thickness, the friction coefficient and asperity capacity for various rolling velocities under the applied load 300 kN/m, both surface roughness amplitude, $R_{rms} = 0.35$ μm, and deviation of the asperity height, $\sigma_s = 0.18$ μm. When rolling velocity increases, the friction coefficient and asperity capacity are decreased to constant value at approximately 2.25 m/s. For the rolling velocity 0.75 m/s, the minimum film thickness, the friction coefficient and asperity capacity are **0.152 μm., 0.3178** and **55.05%**, respectively. When the rolling velocity is increased to 2.25 m/s, the friction coefficient and asperity capacity are decreased to **0.089** and **1.91%**, respectively but the minimum film thickness increase to **0.452 μm.**

The characteristics of mixed lubrication were investigated for non-Newtonian liquid-solid lubricant for various concentration of solid lubricant. When the concentration of solid lubricant was increased, the lubricant film thickness is increased but the friction coefficient and the asperity capacity are decreased as shown in Fig. 5. For pure fluid lubricant under applied load 300 kN/m, rolling velocity 1.25 m/s, both surface roughness amplitude, $R_{rms} = 0.35$ μm, and deviation of the asperity height, $\sigma_s = 0.18$ μm., the minimum film thickness, the friction coefficient and asperity capacity are **0.284 μm., 0.124** and **15.02%**, respectively. When the concentration of solid lubricant is 10.0% by weight, the friction coefficient and asperity capacity are decreased to **0.113** and **11.98%**, respectively but the minimum film thickness is to **0.304 μm.** And the concentration of solid lubricant was 20.0% by weight, the minimum film thickness, the friction coefficient and asperity capacity are **0.325 μm., 0.103** and **9.31%**, respectively.

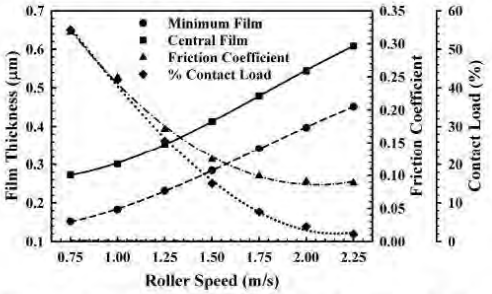

Fig.4 The variation of the lubricant film thickness, the friction coefficient and asperity capacity for various rolling velocity

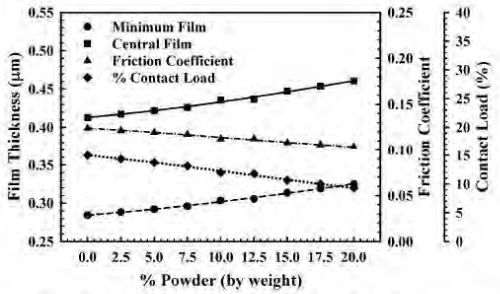

Fig.5 The variation of the lubricant film thickness, the friction coefficient and asperity capacity when various the powder concentration

Conclusion

In this research, the time independent modified Reynolds equation, particle load-carrying equation and Hertzian contact equation were solved to obtain minimum film thickness, friction coefficient and asperity capacity of mixed lubrication in line contact with non-Newtonian liquid-solid lubricant. The following can be concluded as:

1. Considering the rough surface amplitude and applied loads effects, the minimum film thickness decreases but the friction coefficient and asperity capacity increase when amplitude of surface roughness and the applied load are increased.
2. Considering the rolling velocity effect, the minimum film thickness decreases but the friction coefficient and asperity capacity rapidly increase when the rolling velocity is decreased.
3. Considering the solid lubricant effect, the friction coefficient decreases with the concentration of solid particles under mixed lubrication regime. The minimum film thickness increases but the friction coefficient and the asperity capacity decrease when the concentration of solid lubricant is decreased.

Acknowledgment

This paper was supported by grant from Thailand Research Fund; Grant No. BRG-5180019. The additional funding was received through the College of Data Storage Innovation KMITL (DSI – KMITL) and NSTDA for research Unit on Tribology and Mechanical Engineering. The additional support was received through Bangkok University Thailand.

Nomenclature

$E_{1,2}$ Elastic modulus of Plate/ Roller, Pa
E_s Elastic modulus of Solid Lubrication, Pa
E' Effective elastic modulus of Roller/Plate, Pa, $1/E' = 1/\{2[(1-v_1^2)/E_1 + (1-v_2^2)/E_2]\}$
f Friction coefficient
h Lubricant film thickness, m
m_0 Apparent viscosity at the shear rate of unit, Pa-s
n_0 Power law index
n Density of asperity, m^{-2}
p Pressure, Pa
R_2 Radii of curvature of Roller, m
R_1 Radii of curvature of Plate, m
R Curvature sum, m, $1/R = 1/R_1 + 1/R_2$
u Film velocity, m/s
u_1 Plate surface velocity ,m/s
u_2 Roller surface velocity ,m/s
W_T Applied load ,N/m
x Coordinate, m
z Coordinate, m
Z_1 Viscosity-Pressure index
β Radius of asperity, m
μ Equivalent viscosity, Pa-s
μ_0 Inlet viscosity, Pa-s
τ Shear stress of lubricant, Pa
ρ Density of lubricant, kg/m^3
ρ_0 Inlet density of lubricant ,kg/m^3
ρ_p Inlet density of lubricant ,kg/m^3
σ_s Standard deviation of the asperity height distribution, m
λ Concentration by weight of Solid Lubricant

References

[1] D. Dowson and G.R. Higginson : *Elastohydrody-namic Lubrication:The Fundamental of Roller and Gear Lubrication*, Pergamon, Oxford (1966).

[2] M.M. Khonsari, H.S. Wang and Y.L. Qi: *A Theory of Liquid-Solid Lubrication in Elastohydrodynamic Regime*, ASME J. Tribol., vol. 111 (1989), pp. 256-265.

[3] R.S. Sayles and E. Ioannides : *Debris damage in rolling bearings and its effects on fatigue life*, ASME J Tribol ,vol. 110(1988), pp. 26–31.

[4] G.K. Nikas : *Mathematical analysis of the entrapment of solid spherical particles in non-conformal contacts*, ASME J Tribology, Vol. 123(2001), pp.83–93.

[5] A.E. Yousif and S.M. Nacy : *The lubrication of conical journal bearings with bi-phase (liquid–solid) lubricants*, Wear, Vol. 172 (1994), pp. 23–8.

[6] A.A. Lubrecht, W.E. Ten Napel and R. Bosma : *Multi-grid, an Alternative Method for Calculating Film Thickness and Pressure Profiles in EHL Line Contacts*, ASME J. Tribol., Vol. 108 (1986), pp. 551–556.

[7] F.K. Osborn and F. Sadeghi : *Time Dependent Line EHD Lubrication Using the Multigrid/Multilevel Technique*, ASME J. Tribol., Vol. 114 (1992), pp. 68–74.

[8] X. Ai and S.H. Cheng : *Transient EHL Analysis for Line Contacts With Measured Surface Roughness Using Multigrid Technique*, ASME J. Tribol., Vol. 116 (1994) , pp. 549–558.

[9] M. Mongkolwongrojn, C. Aiumpornsin and K. Thammakosol : *Theoretical Investigation in Thermoelastohydrodynamic Lubrication With Non-Newtonian Lubricants Under Sudden Load Change*, Journal of Tribology, vol. 128 (2006), pp. 771–777.

[10] W.Z. Wang, H. Chen, Y.Z. Hu and H. Wang: *Effect of surface roughness parameters on mixed lubrication characteristics*, Tribology International, Vol. 39 (2006), pp 522–527.

[11] C.J.A. Roelands : *Correlational Aspects of the Viscosity-Temperature-Pressure Rela-tionship of Lubricating Oils* , Druk , V.R.B. , Groingen , Netherland (1969)

[12] H.G. Rylander : *A Theory of Liquid-Solid Hydrodynamic Film Lubrication*, ASLE Journal of the American Society of Lubrication Engineerings (1966), pp.264-271.

[13] J.A. Greenwood and J.H. Tripp : *The contact of nominally flat surface*, Proc Inst Mech Eng, Vol 185 (1971), pp. 625–33.

Mechanical Engineering, Materials and Energy
10.4028/www.scientific.net/AMM.148-149

Effect of Liquid-Solid Lubricant on Mixed Lubrication in Line Contact
10.4028/www.scientific.net/AMM.148-149.778

Applied Mechanics and Materials Vols. 148-149 (2012) pp 736-742
Online available since 2011/Dec/22 at www.scientific.net

doi:10.4028/www.scientific.net/AMM.148-149.736

Analysis of Two Surfaces in line contact under TEHL with Non-Newtonian Lubricants

Rattapasakorn Sountaree[1,a] and Mongkolwongrojn Mongkol[2,b]

[1,2] Department of Mechanical Engineering

King Mongkut's Institute of Technology Ladkrabang, Bangkok 10520, THAILAND

[a]sountaree.t@bu.ac.th, [b]kmmongko@kmitl.ac.th

Keywords: TEHL, Non-Newtonian lubricant, Modified Reynolds equation, elastic equation, energy equation, finite difference method with multigrid multilevel technique.

Abstract. This paper presents the static characteristics of two surfaces in line contact under TEHL with non-Newtonian lubricant. Modified Reynolds equation, elastic equation and energy equation were formulated to obtain the model. The model was simulated based on numerical method by using Newton-Raphson and multigrid multilevel techniques. The static characteristics of the two surfaces in line contact under TEHL such as film pressure, film thickness and film temperature profiles in the contact region were examined at various loads, speeds, roller radius and elastic modulus respectively. The results showed the significant effect of load, elastic modulus and surface velocity on the TEHL for machine element operated at severe conditions.

Introduction

Analysis of the lubricating film between metal cylinder and soft cylinder in thermal elastohydrodynamic lubrication problems is important for modern machine components which operated at a very high load and high speed conditions, many of the analyses in EHL problems have used the powerful multigrid multilevel techniques. For example; Dien and Elrod [1] have formulated the time dependent Reynolds equation to obtain the dynamic characteristics of journal bearing with non-Newtonian characteristics assuming constant fluid property in 1983. Wang and Zhang [2] showed the oil film temperature rise and non-Newtonian characteristics of the oil film should be considered in EHL analysis in order to obtain reliable results. These researches are study a behavior of thin film lubricant with focusing on line contact and consider temperature affect of contact surface by using Reynolds equation, film thickness equation, viscosity equation and density equation.

Governing Equations

In this paper, power law model was implemented for the analysis of thermal elastohydrodynamic lubrication with non-Newtonian lubricant. The equivalent viscosity can be approximated as [3]:

$$\mu = m_0 (I)^{\frac{n-1}{2}} \tag{1}$$

Where I = second invariant of strain rate; $I = \left(\frac{\partial u}{\partial z}\right)^2$

Modified Reynolds Equation

The dimensionless modified Reynolds equation for two surfaces in line contact with non-Newtonian lubricant can be expressed as [3]:

$$\frac{\partial}{\partial X}\left(\Phi \frac{\partial P}{\partial X}\right) = K\left(\frac{\partial}{\partial X}(\bar{\rho}H) + \left(\frac{S_X}{2}\right)\frac{\partial}{\partial X}\left(\bar{\rho}H\left(1 - 2\frac{\bar{\mu}_{e0}}{\bar{\mu}_{e1}}\right)\right)\right) \tag{2}$$

Where

$$K=\frac{\overline{u}\,\mu_0 R_X^2}{b^3 P_H},\ \Phi=\overline{\rho}H^3\left(\frac{1}{\overline{\mu}_{e2}}-\frac{\overline{\mu}_{e0}}{\overline{\mu}_{e1}^2}\right)\ \text{and}\ \ \frac{1}{\overline{\mu}_{ei}}=\int_0^1\frac{Z^i}{\overline{\mu}}dZ \tag{3}$$

The boundary conditions are

$$P(X_{IN})=0,\ P(X_{OUT})=\left(\frac{\partial P}{\partial X}\right)_{X=X_{OUT}}=0$$

Viscosity Equation

According to Roeland [4], the viscosity in the power-law model, which depend on pressure, temperature and shear strain in the lubricant shown as

$$\overline{\mu}=\overline{\mu}_P\overline{\mu}_S \tag{4}$$

The term of dimensionless viscosity which change with pressure and temperature as

$$\overline{\mu}_P=\exp\left\{\left[\ln\mu_o+9.67\right]\left[-1+\left(1+5.1\times10^{-9}P_H P\right)^{Z_1}\right]-\gamma T_0\left(\overline{\theta}-1\right)\right\} \tag{5}$$

While the term of dimensionless viscosity which change with shear strain as

$$\overline{\mu}_S=\frac{m_0}{\mu_0}\left(K_{SH}\overline{I}^{\cdot}\right)^{\frac{n-1}{2}} \tag{6}$$

Load balance equation

The load balance equation is

$$\int_{X_{IN}}^{X_{OUT}}PdX=\frac{\pi}{2} \tag{7}$$

Film Thickness Equation

The dimensionless film thickness including deformation of the surfaces can be expressed as

$$H_i=H_0+\frac{X_i^2}{2}+\overline{\delta}_i \tag{8}$$

Where

$$\overline{\delta}_i=-\frac{\Delta X}{2\pi}\sum_{j=0}^{N}P_j\ln\left(\left|\frac{X_{i+1}+X_i}{2}-X_j\right|\left|\frac{X_i+X_{i-1}}{2}-X_j\right|\right) \tag{9}$$

Density Equation

The dimensionless density of a non-Newtonian lubricant from Dowson and Higginson [5] is followed as

$$\overline{\rho}_i=\left(1+\frac{0.6\times10^{-9}P_H P}{1+1.7\times10^{-9}P_H P}\right)\left[1-\beta T_0\left(\overline{\theta}-1\right)\right] \tag{10}$$

Energy Equation

Heat is generated from load that compressed lubricant and shear stress of film lubricant. The dimensionless energy equation of line contact can be expressed as [6]

$$\frac{\partial^2\theta}{\partial Z^2}=K_{T1}\left(\frac{\overline{\rho}H^2}{\overline{k}_P}\right)\left(U\frac{\partial\theta}{\partial X}\right)-K_{T2}\left(\frac{\overline{\mu}}{\overline{k}_P}\right)\left[\frac{\partial U}{\partial Z}\right]^2-K_{T3}\left(\frac{\theta H^2}{\overline{k}_P}\right)\left(U\frac{\partial P}{\partial X}\right) \tag{11}$$

$$\text{Where}\ K_{T1}=\frac{\overline{u}\,\rho_0 C_p b^3}{k_0 R_X^2},\ K_{T2}=\frac{\mu_0\overline{u}^2}{k_0 T_0},\ K_{T2}=\frac{\mu_0\overline{u}^2}{k_0 T_0},\ \overline{k}_P=1+\frac{1.73\text{x}10^{-9}P_H P}{1+6.91\text{x}10^{-10}P_H P} \tag{12}$$

The boundary conditions are

$$\overline{\theta}_{S1/S2}=1+D_{1/2}\int_{X_{IN}}^{X_i}\left(\frac{\overline{k}_P}{H}\right)\left(\frac{\partial\theta}{\partial Z}\right)_{Z=0/1}\frac{dX'}{\sqrt{X_i-X'}},\ D_{1/2}=\frac{k_0 R_X}{\sqrt{\pi\overline{u}\,\rho_{1/2}C_{P,1/2}k_{1/2}b^3\left(1\pm\frac{S_X}{2}\right)}};\ \theta(X=0)=1 \tag{13}$$

Numerical Simulation and Discussion

The research work has investigated the thermoelastohydrodynamic lubrication of two rollers in line contact. Film pressure, film thickness and film temperature of the contact region were obtained at steady state. The mechanical properties of the roller and the property of the non-Newtonian lubricant for the numerical calculation are shown in tables 1.

Table 1 Mechanical properties of the roller and lubricant

Property	Roller	Property	SAE-90
Elasticity modulus, GPa	205	Inlet density, kg/m^3	892.80
Density, kg/m^3	7850	Inlet viscosity, Pa-s	0.1946
Poison ratio	0.30	Power law inlet viscosity, Pa-s	0.1946
Specific heat, J/(kg-K)	475	Flow index (n)	0.9850
Thermal conductivity, W/(m-K)	50.20	Viscosity-Pressure index	0.3917

Results and discussion

The simulation use SAE-90 oil for lubricating between roller 1 and roller 2 which velocity 0.60 and 1.32 m/s respectively.

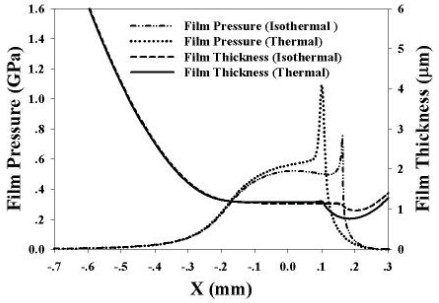

Fig.1 Pressure profile and film thickness profile for EHL for with isothermal and TEHL.

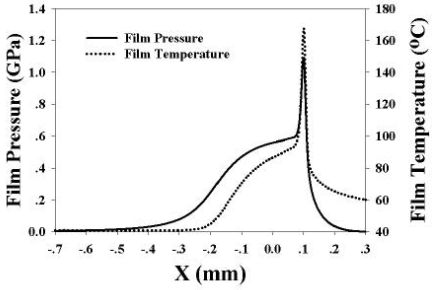

Fig.2 Pressure profile and temperature profile for EHL with isothermal and TEHL.

From figure 1, film pressure and film thickness at the end of contact region are decreased rapidly. The value of pressure for TEHL is higher than that for EHL with isothermal. So, film thickness for TEHL is smaller than that for EHL with isothermal. Figure 2 shows that temperature profile has similar shape to pressure profile.

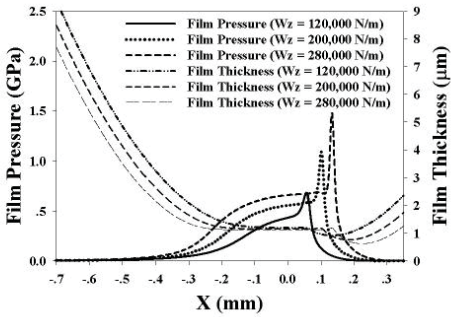

Fig.3 Pressure profile and film thickness profile at various loads.

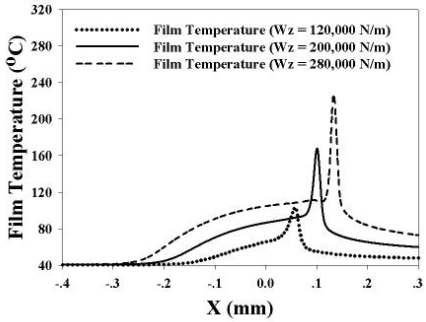

Fig.4 Film temperature profile at various at various loads.

When increase loads from 120,000 N/m to 280,000 N/m, film pressure and film temperature are increased but the film thickness slightly decrease. Pressure and temperature spike increase when loads increase simultaneously as shown in figure 3 and 4.

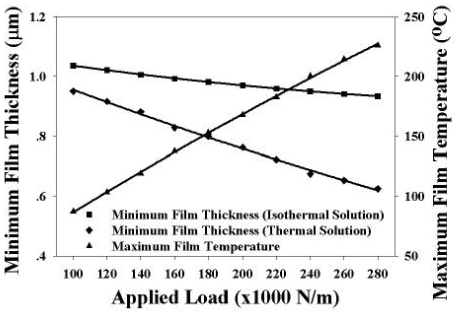

Fig.5 Minimum film thickness and maximum film temperature at various loads.

The relationship between minimum film thickness for EHL with isothermal and the minimum film Film thickness for TEHL are both decrease linearly as load increase but the maximum film temperature increase rapidly and linearly with load as shown in figure 5.

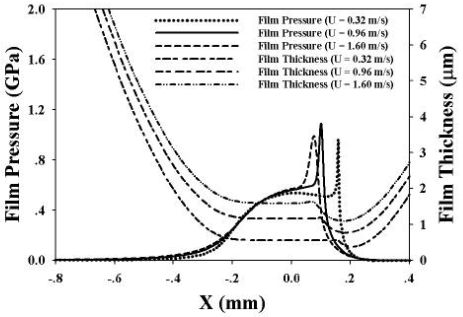

Fig.6 Pressure profile and film thickness profile at various surface velocities of the roller surface

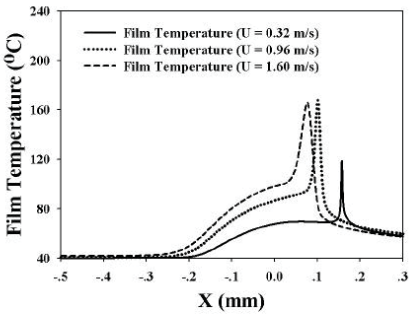

Fig.7 Temperature profile at various velocities of the roller

Figure 6 describes the film pressure and film thickness profiles and figure 7 describes the temperature profile when increase surface velocity of rollers. It can be noted that film thickness and film temperature increase but film pressure still no change.

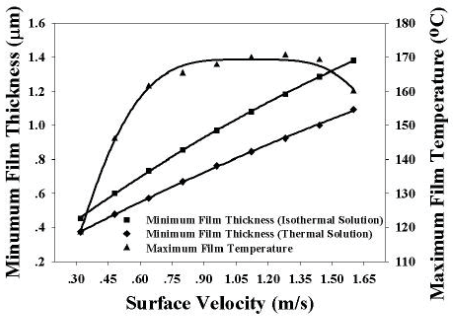

Fig.8 Minimum film thickness and maximum film temperature at various surface velocities of the roller.

Figure 8; shows that for increasing the surface velocity, all the minimum film thickness for EHL with isothermal is higher than the minimum film thickness for TEHL. The difference in minimum film thickness is greater when surface velocity increase. The maximum film temperature increases rapidly for surface velocity form 0.30 to 0.60 m/s and then stay constant until the surface velocity is more than 1.20 m/s.

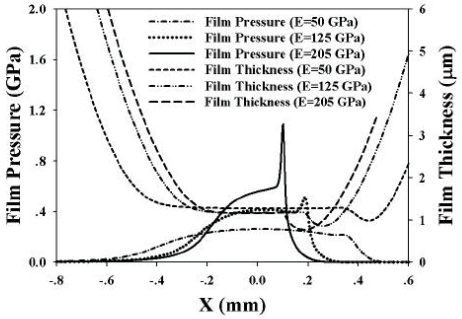

Fig.9 Pressure profile and film thickness profile at various material elastic modulus of the roller.

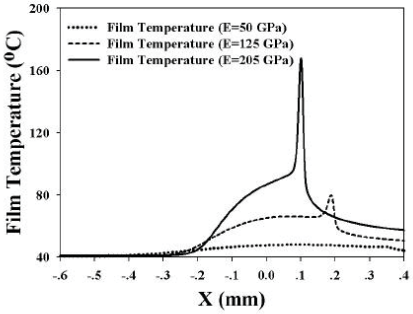

Fig.10 Film temperature profile at various material elastic modulus of the roller.

Figure 9 and 10 show film pressure, film thickness and film temperature profiles for varying the material elastic modulus of roller from 50 GPa to 205 GPa. The pressure profiles show that pressure and pressure spike increase when elastic modulus of roller increase, the film thicknesses decrease slightly. For film temperature, at elastic modulus of rollers 205 GPa, the temperature rise up to 170°C but for roller with low material elastic modulus, the temperature is going up slightly.

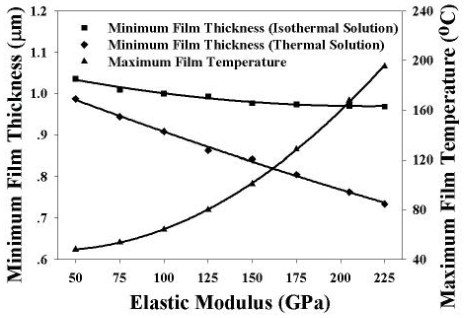

Fig.11 Minimum film thickness and maximum film Temperature at various elastic modulus of rollers

In case of thermoelastohydrodynamic, temperature increases rapidly when increases elastic modulus of roller, the minimum film thickness of isothermal film is greater than the minimum film thickness for TEHL.

Conclusions

The two rollers in line contact under TEHL with non-Newtonian lubricant were examined and can be summarized as:

1. The film pressure and film temperature increase as the applied load increase, but the film thickness decrease slightly.
2. As the surface velocity of rollers increase, the film thickness increase but film temperature decrease slightly specially at high surface velocity.
3. The influence of material elastic modulus of the roller is significant and the film temperature increase with elastic modulus.
4. For roller with lower material elastic modulus, the film temperature increase very small.
5. In the EHL regime, film pressure increase but film thickness decrease due to the temperature in the contact regime under EHL.

Acknowledgment

This paper was supported by grant from Thailand Research Fund; Grant No. BRG – 5180019 and was received through the College of Data Storage Innovation KMITL and NSTDA for research Unit on Tribology and Mechanical Engineering. The additional support was received through Bangkok University Thailand.

Nomenclature

b	Semi-width of Hertzian contact, m
E_1, E_2	Elastic Modulus of Roller, Pa
E'	Equivalent modulus of elasticity, Pa
h	Lubricant film thickness, m
H	Dimensionless film thickness
$\bar{k}_p$	Dimensionless thermal conductivity
K_{SH}	Dimensionless parameter
m_0	Power law inlet viscosity, Pa-s
n	Power law index
p	Film pressure, Pa
P	Dimensionless pressure
P_H	Hertzian's contact pressure, Pa
r_1, r_2	Radius of roller, m
R_X	Radii of curvature, m
S_X	Slip ratio
T	Film temperature, °C
T_0	Inlet film temperature, °C
u_1, u_2	Velocity of roller 1,2, m/s
$\bar{u}$	Mean velocity of roller, m/s,

w_z'	Applied load, N
W'	Dimensionless load
x	Coordinate x-axial, m
X	Dimensionless coordinates,
z	Coordinate z-axial, m
Z	Dimensionless coordinates
ρ	Lubricant density, kg/m^3
ρ_0	Lubricant density at ambient pressure, kg/m^3
$\overline{\rho}$	Dimensionless density
μ_0	Viscosity at ambient pressure, Pa-s
υ_1,υ_2	Poison ratio of cylinder
θ	Dimensionless film temperature
θ_S	Dimensionless surface temperature

References

[1] I.K.Dien and H.G.Elrod: *A Generalized Steady-State for Non-Newtonian fluids, With Application to Journal Bbearing*, Tran. ASME. Journal of Lubrication technology, Vol 105(1983), pp. 385-390.

[2] S.H.Wang and H.H.Zhang: *Combined Effects of Thermal and Non-Newtonian Character of Lubricant on Pressure, Film Profile, Temperature rise, and Shear Stress in E.H.L.*, Tran. ASME. Journal of Tribology, Vol 109(1987), pp. 666-670.

[3] Hua, D. Y. and Khonsari, M. M.: *Elastohydrodynamic Lubrication by Powder Slurries*, *ASME J. Tribology*, Vol 11891996), pp. 67-73.

[4] Roelands,C.J.A.: Correlational Aspects of the Viscosity-Temperature-Pressure Rela-tionship of Lubricating Oils, Druk , V.R.B. , Groingen, Netherland (1969).

[5] Dowson,D., Higginson,G.R.: Elastohy-drodynamic Lubrication:The Fundamental of Roller and Gear Lubrication, Pergamon, Oxford (1966).

[6] Khonsari M.M. and Hua D.Y.: *Thermal Elasto-hydrodynamic Analysis Using a Generalized Non-Newtonian Formulation With Application to Bair-Winer Constitutive Equation*, Tran. ASME. Journal of Tribology, Vol 116(1994), pp. 37-46.

[7] Bernard J. Hamrock: Fundamental of fluid film lubrication, McGraw-Hill, Singapore (1994).

Mechanical Engineering, Materials and Energy
10.4028/www.scientific.net/AMM.148-149

Analysis of Two Surfaces in Line Contact under TEHL with Non-Newtonian Lubricants

10.4028/www.scientific.net/AMM.148-149.736

Tribology International 43 (2010) 1027–1034

Contents lists available at ScienceDirect

Tribology International

journal homepage: www.elsevier.com/locate/triboint

Stability analysis of rough journal bearings under TEHL with non-Newtonian lubricants

Mongkol Mongkolwongrojn *, Chatchai Aiumpronsin

Department of Mechanical Engineering, Faculty of Engineering, King Mongkut's Institute of Technology Ladkrabang, Bangkok 10520, Thailand

ARTICLE INFO

Available online 21 December 2009

Keywords:
Journal bearing
Carreau viscosity model
Surface roughness
Stability analysis
TEHL

ABSTRACT

The combined effects of surface roughness and lubricants rheology on stability of a rigid rotor supported on finite journal bearing under thermal elastohydrodynamic lubrication have been investigated using the transient method. The newly derived time dependent modified Reynolds and the adiabatic energy equations were formulated using a non-Newtonian Carreau viscosity model. The simultaneous systems of modified Reynolds equation, elasticity equation, energy equation, and the rotor motion equation with initial conditions were solved numerically using multigrid multi-level method with full approximation technique. From the characteristic equation, the instability threshold is then obtained with various surface roughness parameters and the elastic modulus of the bearing liner materials. The results show that stability of the bearing system deteriorates with decreasing both the power law exponent and the elastic modulus of bearing liner material. The rough surface journal bearing with transverse pattern under TEHL regime exhibits better stability when compared with the rough surface journal bearing with longitudinal pattern.

1. Introduction

In the design of high speed journal bearings operating under heavy load, the consideration of journal bearing with rough surface in TEHL and flow rheology is significant to predict the stability accurately especially when the film thickness is in the same order as the surface roughness. Few theoretical studies of the journal bearing under elastohydrodynamic lubrication at steady state with Newtonian lubricants are available. Lahmar et al. [1], Mokhimer et al. [2], Taylor and O'Callaghan [3], Oh and Huebner [4], Jain et al. [5] investigated the significant effects of bearing deformation on the bearing performance characteristics with rigid bearing. Thermal effects in thermoelastohydrodynamic (TEHD) lubrication are important due to the strong dependence of viscosity on temperature. Fillon et al. [6,7] and Bouchoule et al. [8] analyzed the TEHD behavior of tilting-pad journal bearings experimentally and theoretically. The comparisons between the theoretical results with experimental data showed that both thermal and the elastic deformation are very important to predict bearing performance. In 2004, Bouyer and Fillon [9] presented the incompressible thermoelastohydrodynamic analysis due to the film pressure which leads to the significant effect on the static characteristics of a plain journal bearing. Transient problems for journal bearing have been studied by numerous investigators. Hashimoto and Mongkolwongrojn [10] studied the dynamic characteristic of turbulent partial journal bearing under hydrodynamic lubrication. Oh and Goenka [11], Van der Tempel et al. [12], Majumdar et al. [13], Prabhakaran Nair et al. [14] and Piffeteau et al. [15] studied the effect of elastic distortion on dynamically loaded journal bearings.

It is now well accepted that the surface roughness and surface pattern has a significant effect on the stability characteristics of hydrodynamic journal bearing. Majumdar and Ghosh [16] analyzed the stability of rough journal bearing using the perturbation technique. Their results shown that the stability improves significantly for a very rough surface bearing with smooth journal surface. Ramesh and Majumdar [17] used the non-linear transient method to show the effects of surface roughness on stability of hydrodynamic journal bearing. Turaga et al. [18], and Gururajan and Prakash [19] studied the influence of the surface roughness on bearing characteristics. Zhang and Cheng [20], and Raghunandana and Majumdar [21] presented the effect of shear thinning fluid on THD of dynamically loaded journal bearing. Kim and Cho [22] developed the 3D average flow model by considering the elastic deformation of pad. And recently, Meng et al. [23] studied the effects of elastic deformation, inter-asperity cavitation and temperature on flow factors.

Modern lubricants contain polymeric additives with shear thinning property. The present study is to incorporate the effects of the shear thinning behavior of lubricant, elastic deformation of the bearing liner, the temperature and pressure dependent

* Corresponding author.
E-mail addresses: kmmongko@kmitl.ac.th (M. Mongkolwongrojn), chataium@gmail.com (C. Aiumpornsin).

0301-679X/$ - see front matter © 2010 Published by Elsevier Ltd.
doi:10.1016/j.triboint.2009.12.039

Nomenclature

A_h	amplitude roughness, m
B	dimensionless damping coefficient
c	bearing radial clearance, m
c_f	specific heat of lubricant, J/(kg K)
e	eccentricity of journal bearing, m
h	oil film thickness, m, $\overline{h}=h/c$
I	second invariant of the strain rate tensor, $I^*=((u_2-u_1)^2+(v_2-v_1)^2)/h^2$
K	dimensionless spring coefficient
m	mass of journal, kg, $M=c\omega^2 m/W$
n	the power law exponent
p	fluid film pressure, Pa
r	journal radius, m
t	time, s, $\tau=\omega_p t$
u	velocity of lubricant in x-direction, m/s
v	velocity of lubricant in y-direction, m/s
x	coordinate in circumferential direction
y	coordinate in axial direction
z	coordinate across fluid film direction
E	elastic modulus of bearing liner, Pa
F_Φ	fluid force component perpendicular to line of center, N
F_R	fluid force component along line of center, N
L	journal bearing length along the axial axis, m
N	rotational speed, rpm
T_m	mean temperature of lubricant across the film, K
T_0	inlet fluid temperature, K
W	resultant fluid force, N
β	coefficient of thermal expansion, 1/K
γ	viscosity–temperature coefficient, 1/K
ρ	density of the lubricant, kg/m^3
ρ_0	density of lubricant at ambient pressure and inlet temperature, kg/m^3
υ	Poisson ratio
Ω	whirl ratio, $\Omega=\omega_p/\omega$
ω	angular velocity of journal, rad/s
ω_p	angular velocity of whirl, rad/s
ε	eccentricity ratio of journal bearing
μ	viscosity, Pa s
μ_0	limiting low shear viscosity, Pa s
μ_∞	limiting high shear viscosity, Pa s
λ	a characteristic relaxation time constant, s
θ	circumferential angle measured from the vertical axis, rad
Φ	attitude angle, rad
λ_l	wave length of roughness, m

characteristics of lubricant viscosity, and the surface roughness of bearing liner in order to analyze the stability of thermal elastohydrodynamic journal bearing. The stability of rough journal bearing was examined using both the perturbation technique and non-linear transient method.

2. Theory

In the present lubrication analysis a full circular journal bearing configuration is considered. The assumptions in the theory of thermal elastohydrodynamic lubrication are:

(1) inertia and body forces of the lubricant are neglected;
(2) both bearing and rotor are rigid;
(3) no slip condition exists;
(4) the fluid flow is laminar;
(5) pressure variation across the film thickness is neglected.

2.1. Reynolds equation

In this research the non-Newtonian lubricant can be approximated using a Carreau viscosity model as

$$\mu=\mu_\infty+(\mu_0-\mu_\infty)(1+\lambda^2 I)^{(n-1)/2} \tag{1}$$

where

$$I=\left(\frac{\partial u}{\partial z}\right)^2+\left(\frac{\partial v}{\partial z}\right)^2 \tag{2}$$

Adopting the perturbation method described by Dien [24], the time dependent modified Reynolds equation with Carreau viscosity model can be formulated as

$$\frac{\partial}{\partial x}\left(\frac{\rho h^3}{\eta}\frac{\partial p}{\partial x}\right)+\frac{\partial}{\partial y}\left(\frac{\rho h^3}{\mu^*}\frac{\partial p}{\partial y}\right)=6\omega r\left(1-\frac{2}{\omega}\dot{\Phi}\right)\frac{\partial \rho h}{\partial x}+12\rho\dot{e}\cos(\theta-\Phi) \tag{3}$$

where

$$\eta=\mu^*+2\left(\frac{u_2-u_1}{h}\right)^2(\mu_0-\mu_\infty)\left(\frac{n-1}{2}\right)\left(1+\lambda^2\left(\frac{u_2-u_1}{h}\right)^2\right)^{(n-3)/2}\lambda^2 \tag{4}$$

$$\mu^*=\mu(I^*)=\mu_\infty+(\mu_0-\mu_\infty)(1+\lambda^2 I^*)^{(n-1)/2} \tag{5}$$

where $x=r\theta$ and boundary conditions are:

$$p(\theta=0)=0,\quad p(y=0)=p(y=L)=0\quad\text{and}\quad p(\theta^*)=\frac{\partial p}{\partial \theta}\Big|_{\theta^*}=0$$

2.2. Energy equation

The mean film temperature of the non-Newtonian Carreau lubricant can be obtained by integrating the energy equation over the film thickness. Assuming adiabatic conditions, the energy equation using Carreau viscosity model can be newly formulated as

$$\begin{aligned}&\left(\rho c_f\frac{u_2}{2}h-\rho c_f\frac{h^3}{12\eta}\frac{\partial p}{\partial x}\right)\frac{\partial T_m}{\partial x}+\left(-\rho c_f\frac{h^3}{12\mu^*}\frac{\partial p}{\partial y}\right)\frac{\partial T_m}{\partial y}\\&=\mu^*\left(\frac{u_2^2}{h}\right)+\left(\beta h T_m\frac{u_2}{2}\right)\frac{\partial p}{\partial x}+\left(\frac{h^3}{12\eta}-\beta T_m\frac{h^3}{12\eta}\right)\left(\frac{\partial p}{\partial x}\right)^2\\&\quad+\left(\frac{h^3}{12\mu^*}-\beta T_m\frac{h^3}{12\mu^*}\right)\left(\frac{\partial p}{\partial y}\right)^2+\beta h T_m\frac{\partial p}{\partial t}-\rho c_f h\frac{\partial T_m}{\partial t}\end{aligned} \tag{6}$$

2.3. Viscosity–pressure–temperature relationship

A general relation proposed by Roelands [25] was used in this study and the viscosity μ^* can be expressed as

$$\mu^*=\mu_0^*\exp\{(\ln\mu_0+9.67)(-1+(1+5.1\times10^{-9}p)^z)-\gamma(T-T_0)\} \tag{7}$$

where μ_0^* is the viscosity at reference temperature and at atmospheric pressure.

2.4. Density–pressure–temperature relationship

The density of lubricant is a function of pressure and temperature and can be determined by a relation proposed by Dowson and Higginson [26].

$$\rho = \rho_0\left(1+\frac{0.6\times10^{-9}p}{1+1.7\times10^{-9}p}\right)(1-\beta(T-T_0)) \tag{8}$$

2.5. Film thickness

The fluid film thickness, h, is determined taking into account the nominal film thickness, roughness height of bush surface, roughness height of journal surface and bush deformation.

$$h = (c+e\cos(\theta-\Phi))-\delta h_1(x,y)+\delta h_2(x,y)+\delta h_D(x,y,p) \tag{9}$$

$\delta h_1(x,y)$ and $\delta h_2(x,y)$ are sinusoid roughness amplitudes of the bush surface and journal surface, respectively. In this study, the journal surface is smooth but the bush surface is a rough surface. $\delta h_1(x,y)$ can be written under the form:

$$\delta h_1(x,y) = A_h\sin\left(\frac{2\pi x}{\lambda_l}\right) \quad \text{(for transverse roughness)} \tag{10}$$

$$\delta h_1(x,y) = A_h\sin\left(\frac{2\pi y}{\lambda_l}\right) \quad \text{(for longitudinal roughness)} \tag{11}$$

$\delta h_D(x,y,p)$ is the bush deformation as described by Dobrica Mihai et al. [27]. For a discrete domain having M × N equally sized elements, the relation between local displacement and pressure field is given by Eq. (12):

$$\delta h_D(x,y,p) = \frac{1-\upsilon^2}{\pi E}\sum_{k=1}^{M}\sum_{l=1}^{N}\int_{y_l-\Delta y/2}^{y_l+\Delta y/2}\int_{x_k-\Delta x/2}^{x_k+\Delta x/2}\frac{dx\,dy}{\sqrt{(x_l-x)^2+(y_j-y)^2}}p_{k,l} \tag{12}$$

2.6. Load-carrying capacity

The thermoelastohydrodynamic forces on journal bearing in vertical (F_ξ) and horizontal (F_ψ) direction can be expressed as

$$F_\xi = -\int_0^L\int_0^{\theta''} p\cos\theta r\,d\theta\,dy \tag{13}$$

$$F_\psi = -\int_0^L\int_0^{\theta''} p\sin\theta r\,d\theta\,dy \tag{14}$$

The forces in vertical and horizontal direction can be converted to the forces in radial direction (F_r) and the circumferential direction (F_Φ) as

$$F_r = -F_\xi\cos\Phi - F_\psi\sin\Phi \tag{15}$$

$$F_\Phi = F_\xi\sin\Phi - F_\psi\cos\Phi \tag{16}$$

The total load capacity (W) and the attitude angle (Φ) are:

$$W = (F_r^2+F_\Phi^2)^{1/2} \tag{17}$$

$$\Phi = \tan^{-1}\left(-\frac{F_\Phi}{F_r}\right) \tag{18}$$

2.7. Equation of motion

According to Turaga et al. [28], the equation of motion for a balanced rigid rotor of dimensionless mass M, can be written as

$$M\Omega^2\left[\frac{d^2\varepsilon}{d\tau^2}-\varepsilon\left(\frac{d\Phi}{d\tau}\right)^2\right] = \frac{F_r+W\cos\Phi}{W} \tag{19}$$

$$M\Omega^2\left[\varepsilon\frac{d^2\Phi}{d\tau^2}+2\frac{d\varepsilon}{d\tau}\frac{d\Phi}{d\tau}\right] = \frac{F_\Phi-W\sin\Phi}{W} \tag{20}$$

2.8. Linearization of bearing reaction

According to Lund theory [29], the steady-state pressure and the perturbed pressure for horizontal and vertical coordinates, ξ–ψ direction, can be obtained as

$$\left[\frac{1}{r^2}\frac{\partial}{\partial\theta}\left(\frac{\rho h_s^3}{12\eta}\frac{\partial}{\partial\theta}\right)+\frac{\partial}{\partial y}\left(\frac{\rho h_s^3}{12\mu^*}\frac{\partial}{\partial y}\right)\right]\begin{Bmatrix}p_s\\p_\xi\\p_\psi\\p_{\dot\xi}\\p_{\dot\psi}\end{Bmatrix} = \begin{Bmatrix}\dfrac{U}{2r}\dfrac{\partial\rho h_s}{\partial\theta}\\ \dfrac{U}{2r}\dfrac{\partial(\rho\cos\theta)}{\partial\theta}-\dfrac{1}{r^2}\dfrac{\partial}{\partial\theta}\left(\dfrac{\rho h_s^2\cos\theta}{4\eta}\dfrac{\partial p_s}{\partial\theta}\right)-\dfrac{\partial}{\partial y}\left(\dfrac{\rho h_s^2\cos\theta}{4\mu^*}\dfrac{\partial p_s}{\partial y}\right)\\ \dfrac{U}{2r}\dfrac{\partial(\rho\sin\theta)}{\partial\theta}-\dfrac{1}{r^2}\dfrac{\partial}{\partial\theta}\left(\dfrac{\rho h_s^2\sin\theta}{4\eta}\dfrac{\partial p_s}{\partial\theta}\right)-\dfrac{\partial}{\partial y}\left(\dfrac{\rho h_s^2\sin\theta}{4\mu^*}\dfrac{\partial p_s}{\partial y}\right)\\ \rho\cos\theta\\ \rho\sin\theta\end{Bmatrix} \tag{21}$$

where $p_s=(p)_s$, $p_\xi=(\partial p/\partial\xi)_s$, $p_\psi=(\partial p/\partial\psi)_s$, $p_{\dot\xi}=(\partial p/\partial\dot\xi)_s$, $p_{\dot\psi}=(\partial p/\partial\dot\psi)_s$

$$h = h_s+\Delta\xi\cos\theta+\Delta\psi\sin\theta \tag{22}$$

$$h_s = (c+e\cos(\theta-\Phi))-\delta h_1(x,y)+\delta h_2(x,y)+\delta h_D(x,y,p) \tag{23}$$

The dimensionless spring and damping coefficients can be obtained as followings

$$\begin{Bmatrix}K_{\xi\xi} & K_{\xi\psi}\\ K_{\psi\xi} & K_{\psi\psi}\end{Bmatrix} = \frac{c}{W}\begin{Bmatrix}-\int_0^L\int_0^{2\pi}p_\xi r\cos\theta\,d\theta\,dy & -\int_0^1\int_0^{2\pi}p_\psi r\cos\theta\,d\theta\,dy\\ -\int_0^1\int_0^{2\pi}p_\xi r\sin\theta\,d\theta\,dy & -\int_0^L\int_0^{2\pi}p_\psi r\sin\theta\,d\theta\,dy\end{Bmatrix} \tag{24}$$

$$\begin{Bmatrix}B_{\xi\xi} & B_{\xi\psi}\\ B_{\psi\xi} & B_{\psi\psi}\end{Bmatrix} = \frac{c\omega}{W}\begin{Bmatrix}-\int_0^L\int_0^{2\pi}p_{\dot\xi} r\cos\theta\,d\theta\,dy & -\int_0^1\int_0^{2\pi}p_{\dot\psi} r\cos\theta\,d\theta\,dy\\ -\int_0^1\int_0^{2\pi}p_{\dot\xi} r\sin\theta\,d\theta\,dy & -\int_0^L\int_0^{2\pi}p_{\dot\psi} r\sin\theta\,d\theta\,dy\end{Bmatrix} \tag{25}$$

The solutions for critical mass and whirl ratio are:

$$\Omega^2 M_{CR} = \frac{B_{\xi\xi}K_{\psi\psi}+B_{\psi\psi}K_{\xi\xi}-B_{\psi\xi}K_{\xi\psi}-B_{\xi\psi}K_{\psi\xi}}{B_{\xi\xi}+B_{\psi\psi}} \tag{26}$$

$$\Omega^2 = \frac{(K_{\xi\xi}-\Omega^2M_{CR})(K_{\psi\psi}-\Omega^2M_{CR})-K_{\xi\psi}K_{\psi\xi}}{B_{\xi\xi}B_{\psi\psi}-B_{\xi\psi}B_{\psi\xi}} \tag{27}$$

3. Results and discussion

In the present study, a full circular journal bearing configuration is considered and the detail information about physical properties of journal bearing and physical properties of the lubricant are given in Tables 1 and 2, respectively. Thermoelastohydrodynamic lubrication in journal bearing with non-Newtonian Carreau viscosity fluid is used to study the effects of roughness and elastic modulus of bearing liner material. The

surface roughness of the bearing liner in this research work is a harmonic function with 5000 μm in wave length. The dynamic characteristics of a finite length full circular journal bearing with L/D = 1 are analyzed using both linear and non-linear methods as shown in Figs. 1–5.

Table 1
Physical properties of journal bearing.

Journal radius, r	0.015 m
Bearing length, L	0.030 m
Radius clearance, c	30 μm
Rotational speed, N	3000 rpm
Material elastic modulus of bearing liner, E	70 GPa, 200 GPa
Poisson ratio of bearing, υ	0.3
Wave length of roughness, λ_1	0.005 m

Table 2
Physical properties of the lubricant.

Lubricant type	SAE 10W50
Limiting viscosity at low shear rate, μ_0	0.107 Pa s
Limiting viscosity at high shear rate, μ_∞	0.054 Pa s
Power-law exponent, n	0.341
Characteristic relaxation time constant, λ	3.0E−06
Lubricant density, ρ	875 kg/m^3
Lubricant specific heat, c_r	1900 J/kg K
Inlet lubricant temperature, T_0	313 K
Viscosity–pressure index, Z	0.60
Viscosity–temperature coefficient, γ	0.0310174 K^{-1}
Coefficient of thermal expansivity, β	0.000788 K^{-1}

The fluid film stiffness coefficients and the damping coefficients of journal bearing lubricated with non-Newtonian Carreau viscosity model with roughness surface are shown in Figs. 1 and 2, respectively. The spring coefficients increase as the roughness amplitude increase but damping coefficients decrease with the increasing in roughness amplitude for transverse roughness pattern. Fig. 3 shows the influences of bearing liner roughness on the region of stability. It can be noted that the journal bearing is highly stable with higher roughness amplitude for transverse pattern specially for elastic modulus of E=200 GPa due to an increase in fluid film stiffness, reduction in the fluid film damping with increasing amplitude roughness.

In this paper, the combined effects of journal bearing with rough surfaces under thermal elastohydrodynamic lubrication and non-Newtonian lubricants based on Carreau model on rotor stability are examined by a non-linear transient method. The trajectories of the journal center of the finite journal bearing with 3 μm in transverse surface roughness amplitude at load W = 8 kN and mass parameter $M\Omega^2$ = 3.5 under thermal elastohydrodynamic lubrication for E = 200 GPa is compared with the trajectories of the journal center under thermal elastohydrodynamic lubrication for E = 70 GPa as shown in Figs. 4 and 5. The effect of journal bearing with soft material; E = 70 GPa; the journal center trajectory occur with the maximum distance more than 1.0 for transverse roughness surface in Fig. 4 and with the distance equal to 1.0 for longitudinal roughness surface in Fig. 5, the journal center trajectory has clearly observed a decrease in stability for both surface patterns. By comparing Fig. 4 with Fig. 5, the results show that the journal bearings with transverse surface roughness improve the stability.

The effects of L/D ratio on dynamic characteristics of journal bearing under thermoelastohydrodynamic lubrication with

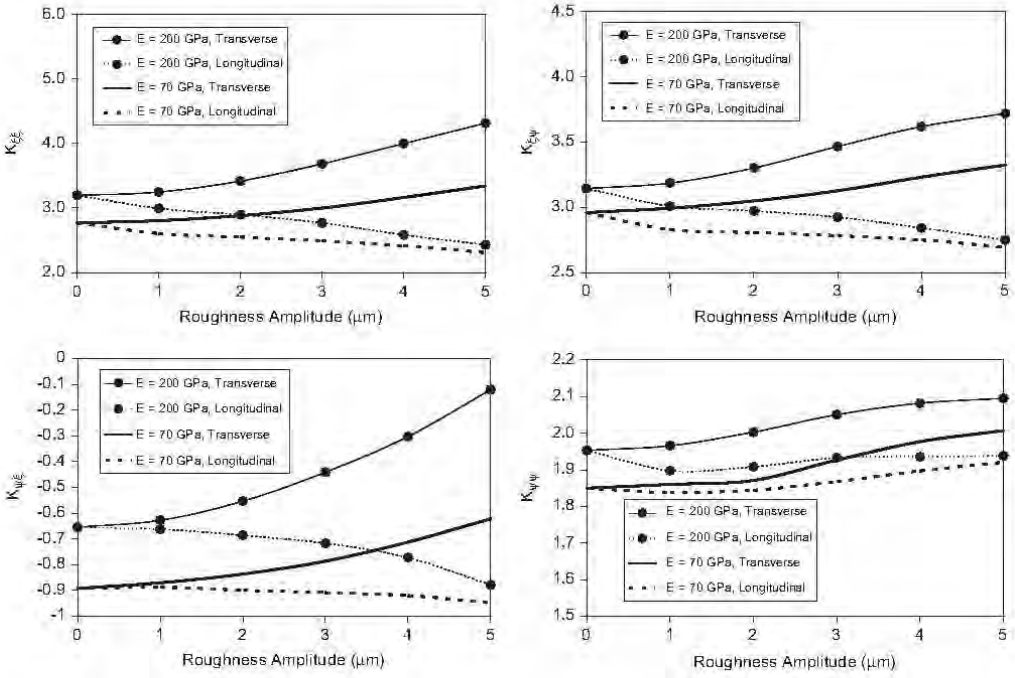

Fig. 1. Variation of dimensionless spring coefficients when journal bearing operated at a speed of 3000 rpm and an eccentricity ratio of 0.8.

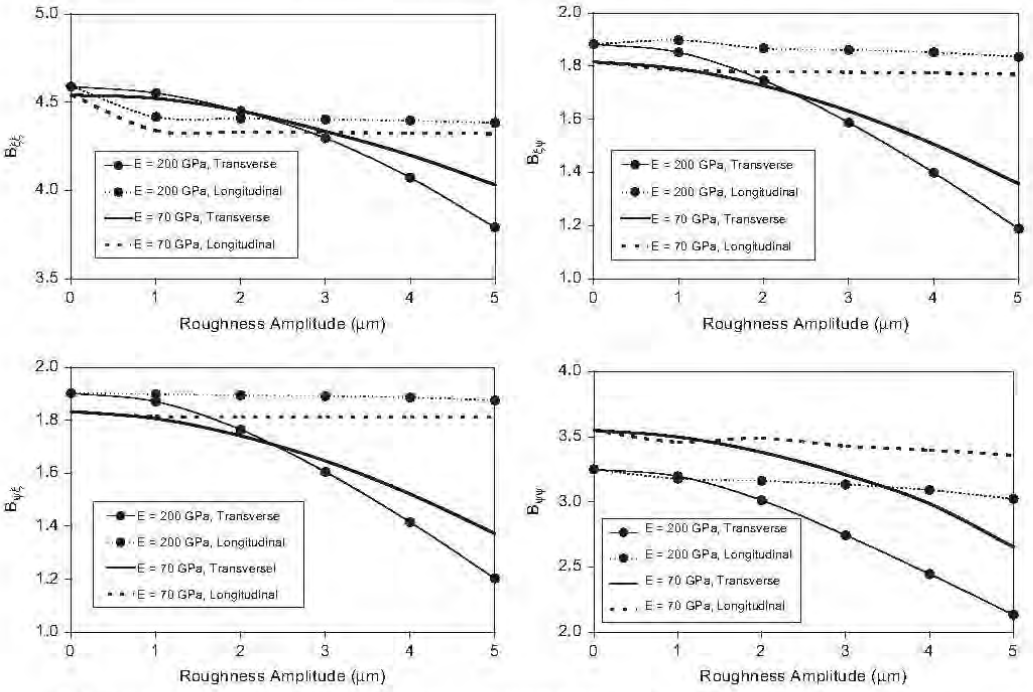

Fig. 2. Variation of dimensionless damping coefficients when journal bearing operated at a speed of 3000 rpm and an eccentricity ratio of 0.8.

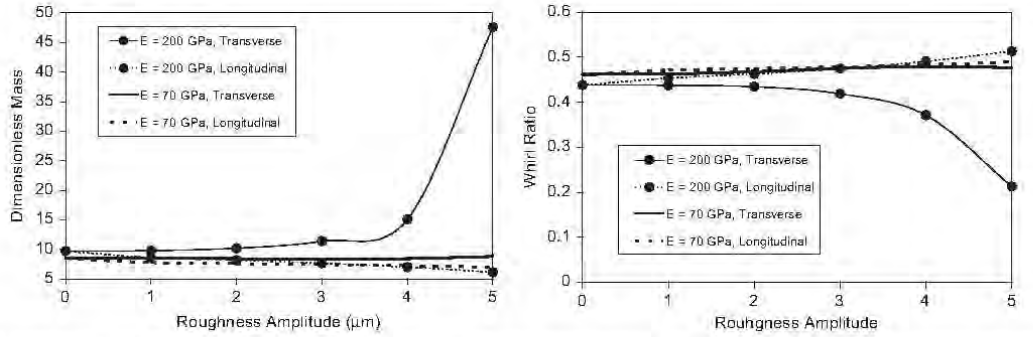

Fig. 3. Variation of dimensionless mass and whirl ratio with roughness amplitude when journal bearing operated at a speed of 3000 rpm and an eccentricity ratio of 0.8.

non-Newtonian Carreau viscosity model are analyzed as shown in Fig. 6. The journal bearing operate with rough surface bearing liner; 5 μm in amplitude and 5000 μm in wave length, operates at eccentricity ratio equal to 0.8. The results show that the stability region becomes better when L/D is small and the stability decrease as L/D increase. Transverse roughness pattern gives better stability characteristic than the stability of the journal bearing with longitudinal roughness pattern. The elastic modulus of bearing liner and longitudinal roughness pattern has no effect on the stability of journal bearing when L/D ratio was more than 1.5.

The combined effects of surface roughness and power law index on dynamic characteristics of the journal bearing under thermoelastohydrodynamic lubrication with non-Newtonian Carreau viscosity lubricant and elastic modulus of bearing liner E=70 GPa are analyzed as shown in Figs. 7–9. The finite journal bearing operate at eccentricity ratio equal to 0.8 and the bearing liner with various transverse surface roughness. The results show that the stiffness coefficients increase significantly when the surface roughness of bearing liner is increased but the stiffness coefficients increase slightly as the power law index is increased as shown in Fig. 7. The damping

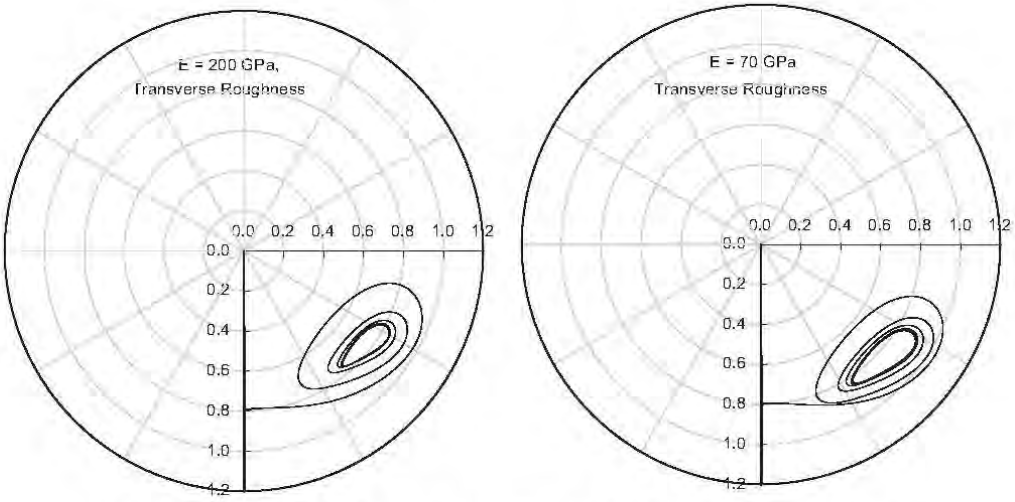

Fig. 4. Journal center trajectory under TEHL with transverse roughness surface, when load W=8 kN, mass parameter $M\Omega^2$=3.5.

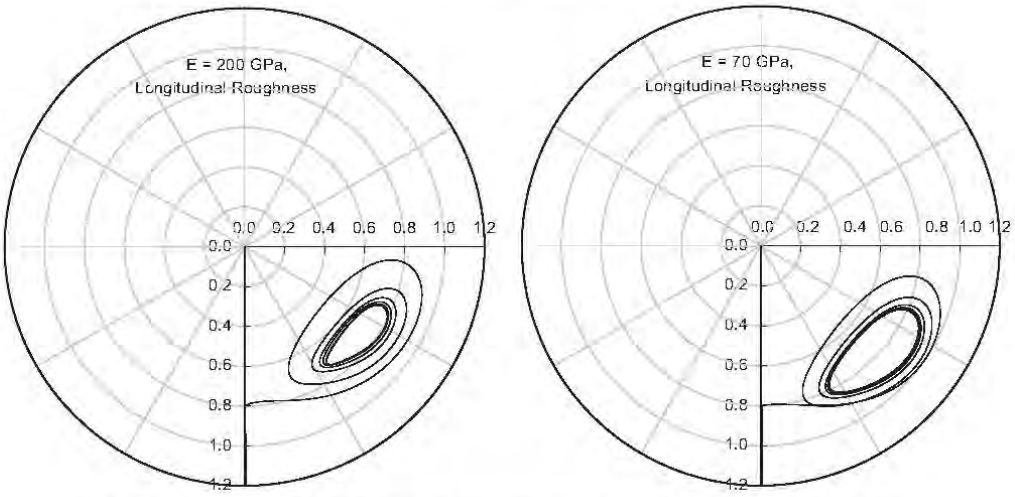

Fig. 5. Journal center trajectory under TEHL with longitudinal roughness surface, when load W=8 kN, mass parameter $M\Omega^2$=3.5.

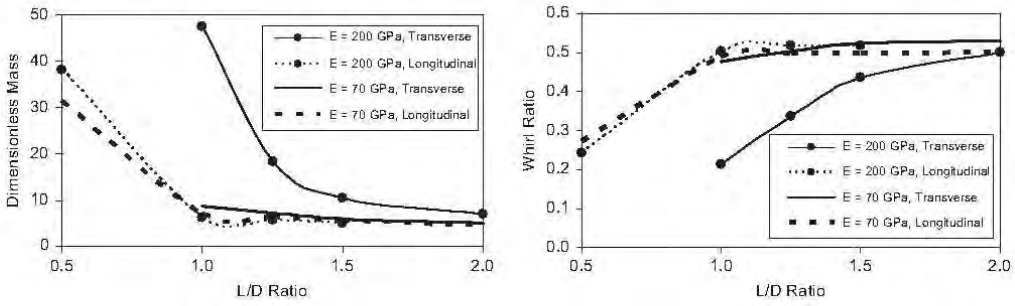

Fig. 6. Variation of dimensionless mass and whirl ratio with L/D ratio when journal bearing operated at a speed of 3000 rpm, eccentricity ratio=0.8, and roughness amplitude=5 μm.

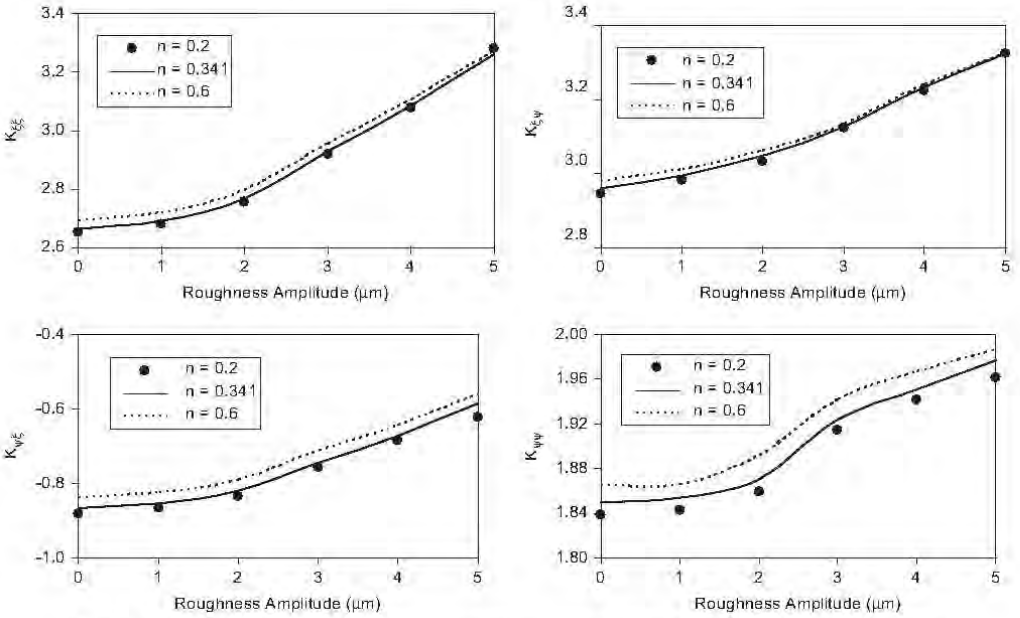

Fig. 7. Effects of power law index and transverse roughness amplitude on spring coefficients for eccentricity ratio=0.8 and E=70 GPa.

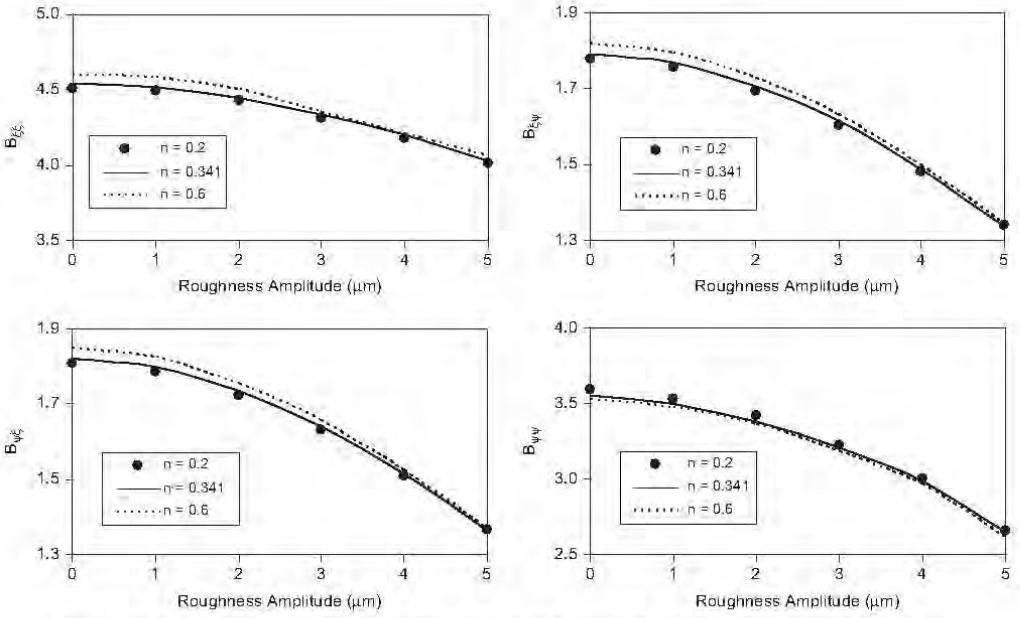

Fig. 8. Effects of power law index and transverse roughness amplitude on damping coefficients for eccentricity ratio=0.8 and E=70 GPa.

coefficients decrease significantly when the surface roughness of bearing liner is increased but the stiffness coefficients increase slightly as the power law index is increased as shown in Fig. 8. The stability improves marginally with an increase in power law index as well as with an increase in transverse surface roughness.

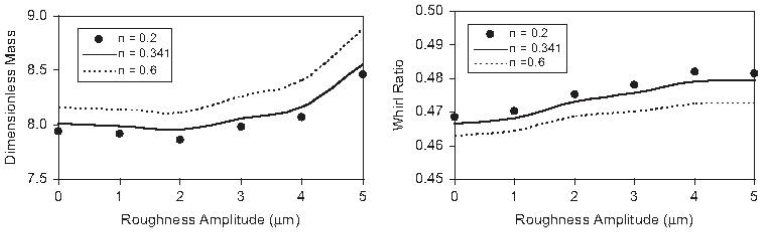

Fig. 9. Effects of power law index and transverse roughness amplitude on dimensionless mass and whirl ratio at eccentricity ratio=0.8 and E=70 GPa.

4. Conclusions

The influence of surface roughness and material modulus on the dynamic characteristics of the journal bearing under thermal elastohydrodynamic lubrication with non-Newtonian Carreau viscosity model are examined theoretically and can be concluded as:

(1) the time dependent modified Reynolds equation and the adiabatic energy equation with non-Newtonian Carreau viscosity model are formulated and solved numerically using Newton method and multigrid multi-level with full approximate scheme techniques;
(2) for journal bearing under thermal elastohydrodynamic lubrication operated at severe conditions, the journal bearing with transverse surface roughness pattern in the bearing liner exhibit better stability, specially for bearing liner with high surface roughness amplitude and the region of stability decreases for the bearing liner with lower elastic modulus material;
(3) for bearing liner with transverse surface roughness pattern, the stability of the journal bearing under thermal elastohydrodynamic lubrication increase significantly as bearing L/D ratio is decreased;
(4) for journal bearing under thermal elastohydrodynamic lubrication operated at severe conditions, the stability region increases with an increase of power law index.

Acknowledgment

This paper was supported by a grant from Thailand Research Fund Grant No. BRG-5180019. The additional funding was received through the DSTAR-KMITL and NSTDA for Research Unit on Tribology and Mechanical Engineering.

References

[1] Lahmar M, Haddad A, Nicolas D. Elastohydrodynamic analysis of one-layered journal bearings. Journal of Engineering Tribology, Proceedings of the Institution of Mechanical Engineers 1998;212(Part J):193–205.
[2] Mokhiamer UM, Crosby WA, El-Gamal HA. A study of a journal bearing lubricated by fluid with couple stress considering the elasticity of the liner. Wear 1999;224:194–201.
[3] Taylor C, O'Callaghan JFA. Numerical solution of the elastohydrodynamic problem using finite elements. Journal of Mechanical Engineering and Science 1972;14:229–36.
[4] Oh KP, Huebner KH. Solution of the elastohydrodynamic finite journal bearing problem. ASME Journal of Lubrication Technology 1973;95(3):342–52.
[5] Jain SC, Sinhasan R, Singh DV. A study of EHD lubrication in a journal bearing with piezoviscous lubricants. ASLE Transaction 1984;27:168–76.
[6] Fillon M, Souchet D, Frêne J. Influence of bearing element displacements on thermohydrodynamic characteristics of tilting-pad journal bearing. Proceedings of the Japan international tribology conference, ITC Nagoya'90; 1990. p. 635–40.
[7] Fillon M, Bligoud JC, Frêne J. Experimental study of tilting-pad journal bearings—comparison with theoretical thermoelastohydrodynamic results. ASME Journal of Tribology 1992;11:579–88.
[8] Bouchoule C, Fillon M, Nichoas D, Barresi F. Experimental study of thermal effects in tilting-pad journal bearings at high operating speeds. ASME Journal of Tribology 1996;118:532–8.
[9] Bouyer J, Fillon M. On the significance of thermal and deformation effects on a plain journal bearing subjected to severe operating conditions. ASME Journal of Tribology 2004;126:819–22.
[10] Hashimoto H, Mongkolwongrojn M. Adiabatic approximate solution for static and dynamic characteristics of turbulent partial journal bearings with surface roughness. ASME Journal of Tribology 1994;116:672–80.
[11] Oh KP, Goenka PK. The elastohydrodynamic solution of journal bearing under dynamic loading. ASME Journal of Tribology 1985;107:389–95.
[12] Van der Tempel L, Moes H, Bosma R. Numerical simulation of dynamically loaded flexible short journal bearings. ASME Journal of Tribology 1985 396–401.
[13] Majumdar BC, Brewe DE, Khonsari MM. Stability of a rigid rotor supported on flexible oil journal bearings. ASME Journal of Tribology 1988;110:181–7.
[14] Prabhakaran Nair K, Sukumaran Nair VP, Jayadas NH. Static and dynamic analysis of elastohydrodynamic elliptical journal bearing with micropolar lubricant. Tribology International 2007;40:297–305.
[15] Piffeteau S, Souchet D, Bonneau D. Influence of thermal and elastic deformations on connecting-rod big end bearing lubrication under dynamic loading. ASME Journal of Tribology 2000;122:181–91.
[16] Majumdar BC, Ghosh MK. Stability of a rigid rotor supported on rough oil jornal bearign. ASME Journal of Tribology 1990;112:73–7.
[17] Ramesh J, Majumdar BC. Stability of rough journal bearings using nonlinear transient method. ASME Journal of Tribology 1995;117:691–5.
[18] Turaga R, Sekhar AS, Majumdar BC. The effect of roughness parameter on the performance of hydrodynamic journal bearings with rough surfaces. Tribology International 1999;32:231–6.
[19] Gururajan K, Prakash J. Surface roughness effects in infinitely long porous journal bearing. ASME Journal of Tribology 1999;121:139–47.
[20] Zhang Ch, Cheng HS. Transient non-Newtonian thermo-hydrodynamic mixed lubrication of dynamically loaded journal bearing. ASME Journal of Tribology 2000;122:156–61.
[21] Raghunandana K, Majumdar BC. Stability of journal bearing systems using non-Newtonian lubricants: a non-linear transient analysis. Tribology International 1999;32:179–84.
[22] Kim TW, Cho YJ. Average flow model with elastic deformation for CMP. Tribology International 2006;39:1388–94.
[23] Meng FM, Cen SQ, Hu YZ, Wang H. On elastic deformation, inter-asperity cavitation and lubricant thermal effect on flow factors. Tribology International 2009;42:260–74.
[24] Dien IK, Elrod HG. A generalized steady-state reynolds equation for non-Newtonian fluids, with application to journal bearings. ASME Journal of Lubrication Technology 1983;105:385–90.
[25] Roelands CJA. Correlational aspects of the viscosity-temperature-pressure relationship of lubricating oils. PhD thesis, Technical University of Delft, The Netherlands; 1966.
[26] Dowson D, Higginson GR. Elastohydrodynamic lubrication: the foundamentals of roller and gear lubrication. Oxford, UK: Pergamon; 1966.
[27] Dobrica Mihai B, Fillon M, Maspeyrot P. Mixed elasto-hydrodynamic lubrication in a partial journal bearing—comparison between deterministic and stochastic models. ASME Journal of Tribology 2006;128:778–88.
[28] Turaga R, Sekhar AS, Majumdar BC. Comparison between linear and nonlinear transient analysis techniques to find the stability of a rigid rotor. ASME Journal of Tribology 1999;121:198–201.
[29] Lund JW. Review of the concept of dynamic coefficients for fluid film journal bearings. ASME Journal of Tribology 1987;109:37–41.

Journal of Template

Vol. 00, No. 0, 0000

Effect of Solid Lubricant Particles on Rough Thermal Elastohydrodynamic Lubrication in Spur Gears *

Mongkolwongrojn, Mongkol** and Panichakorn, Jesda**
** Department of Mechanical Engineering, Faculty of Engineering,
King Mongkut's Institute of Technology Ladkrabang, Bangkok 10520, Thailand
E-mail: kmmongko@kmitl.ac.th

Abstract
This paper presents the performance characteristics of rough surface spur gears under thermo-elastohydrodynamic lubrication (TEHL) with non-Newtonian liquid–solid lubricant based on a Power law viscosity model. The time dependent modified Reynolds equation, elasticity equation, powder load carrying capacity, and energy equation with initial conditions were formulated and solved numerically using a multigrid multilevel with full approximation technique for an involute spur gear. In this analysis, the normal load and overloads are applied on either two pairs or one pair of gear teeth. The transitions from two pairs to one pair and vice versa are modeled as a step variation of load. The effects of powder concentration, diameter of solid particle, surface roughness, and non-Newtonian lubricant properties were examined in the region along the line of action of the meshing gear. The results show that the powder concentration and surface roughness affect significantly the film thickness, film temperature and friction coefficient, but the diameters of solid particle are relatively insignificant for rough TEHL.

Key words: Liquid-Solid lubricant, Rough surface, TEHL, Spur gear

1. Introduction

The TEHL analysis of involute spur gears is a non-stationary problem. It is very hard to predict the film thickness and film temperature of the lubricant in contact region. In this case, it is not only the load that varies, but entrainment velocity and contact geometry also vary as the gear teeth come into action. Moreover, the surface roughness of gear teeth, high shear stress behavior of the liquid-solid lubricant properties and the load all vary significantly along the line of action. So it is very hard to get all these effects into a transient thermo-elastohydrodynamic solution for an involute spur gear.

The gear problem has historically been solved with different simplifications. The numerical solution of elastohydrodynamic lubrication (EHL) problems was described by Dowson and Higginson[1]. Many numerical solutions have been obtained in the area ranging from thermo-elastohydrodynamic (TEHD) lubrication problems to transient TEHL problems. Wang and Cheng [2,3] made a Grubin-type analysis of involute spur gear transmissions and were able to calculate the minimum film thickness at several points along the line of action. Hua and Khonsari[4] gave an isothermal full transient solution for involute spur gear by neglecting dynamic load in the model. Later, a full isothermal transient non-Newtonian EHL solution to the Reynolds equation was given by Larsson[5]. Wang[6] presented the formulation of the transient TEHL problem in spur gears. The results showed that the transient condition affects significantly the film temperature and film

*Received XX Xxx, 200X (No. XX-XXXX)
[DOI: 00.0000/ABCDE.2006.000000]

thickness of lubricant in the contact region. Mongkolwongrojn and Panichakorn[7] studied TEHL rough surface spur gears under sudden overloads. The results showed that the effects of sudden overloads are significant for the friction coefficient, the film temperature and film thickness of lubricant in the contact region. Sayles [8] came to the conclusion that particles larger than the oil film thickness and softer than the interacting surfaces would also hurt the surface, and reduce the life of the tribopair. Khonsari, Wang, and Qi[9] formulated Reynolds and energy equations for non-Newtonian liquid-solid lubricants in line contact. Yousif [10] obtained the improved lubrication characteristics by mixing soft MoS2 and graphite particles with pure oil. Mongkolwongrojn[11] showed that the liquid-solid non-Newtonian lubricant affects significantly the film temperature and film thickness of lubricant in contact region under sudden load. Lubrecht, Ten Napel, and Bosma [12] showed that the multigrid algorithm is the most efficient method for solving the highly nonlinear EHL problems with roughness effects. The multigrid technique has been developed to solve transient thermo-elastohydrodynamic lubrication (TEHL) by Osborn and Sadeghi [13]. Ai and Cheng[14] presented the formulation of the transient rough EHL problem using a multigrid technique. The results showed that surface roughness affects significantly the transient pressure distribution in line contact. Wang[15] presented a technique to generate non-Gaussian surfaces for mixed lubrication.

In the present analysis, rough spur gears with liquid-solid non-Newtonian lubricant is incorporated in TEHL analysis. Gear teeth with rough surfaces are assumed in this full transient thermal EHL analysis. Finite difference multigrid multilevel method with full approximate scheme techniques were implemented to calculate the transient TEHD lubrication of rough surface gear teeth with various particle materials and various percent of particle concentration for the liquid-solid non-Newtonian lubricants. Minimum film thickness, maximum film temperature and friction coefficient were determined at different contact points along the line of action.

Nomenclature

b : Semi-width of Hertzian contact under loadw_0', m, $b = R_0(8W_0'/\pi)^{1/2}$
C_{RT} : Transient dimensionless curvature sum, $C_{RT} = R_X/R_0$
C_{UT} : Transient dimensionless entrainment velocity, $C_{RT} = \bar{u}/u_0$
C_{WT} : Transient dimensionless load, $C_{WT} = w'/w_0'$
$D(X)$: Dimensionless of combined surface roughness of gear and pinion
$E_{1/2}$: Elastic modulus of pinion/gear, Pa
E_s : Elastic modulus of Solid Lubrication, Pa
E' : Effective elastic modulus, Pa, $1/E' = 1/\{2[(1-v_1^2)/E_1 + (1-v_2^2)/E_2]\}$
f : Friction coefficient of pinion
f_p : Friction coefficient of solid lubricant particle
h : Lubricant film thickness, m
h_0 : Rigid central film thickness, m
H : Dimensionless film thickness, $H = h(R_0/b^2)$
H_0 : Dimensionless rigid central film thickness, $H_0 = h_0(R_0/b^2)$
K : Constant in Reynolds equation
k : Thermal conductivity of lubricant, W/m · K
k_0 : Thermal conductivity of lubricant at ambient pressure, W/m · K
$\bar{k}_P$: Dimensionless Thermal conductivity of lubricant $\bar{k}_P = k/k_0$
K_{T1} : Constant in Energy equation
K_{T2} : Constant in Energy equation
K_{T3} : Constant in Energy equation
m_0 : Apparent viscosity at the shear rate of unit, Pa · s

n : Power law index
p : Pressure, Pa
P : Dimensionless pressure, $P = p/P_H$
P_H : Maximum Hertzian pressure, Pa, $P_H = E'(W_0'/2\pi)^{1/2}$
r_a : Base cycle radii of pinion, m
r_b : Base cycle radii of gear, m
R_0 : Pitch circle radii sum, m, $1/R_0 = 1/r_a\sin(\bar{\varphi}) + 1/r_b\sin(\bar{\varphi})$
R_1 : Radii of curvature of pinion teeth, m
R_2 : Radii of curvature of gear teeth, m
R_X : Curvature sum, m, $1/R_X = 1/R_1 + 1/R_2$
$\bar{S}$: Distance along line of action, m
S_0 : Slip ratio, $S_0 = (u_2 - u_1)/\bar{u}$
t : Time, s
$\bar{t}$: Dimensionless time, $\bar{t} = t(u_o/b)$
T : Temperature, K
T_1 : Surface temperature of pinion, K
T_2 : Surface temperature of gear, K
T_0 : Inlet temperature, K
u : Film velocity, m/s
u_1 : Pinion teeth surface velocity, m/s
u_2 : Gear teeth surface velocity, m/s
$\bar{u}$: Entrainment velocity, m/s,$\bar{u} = (u_2 + u_2)/2$
u_0 : Reference velocity, m/s
u^* : Dimensionless film velocity,$u^* = u/u_0$
w' : Transient load, N/m
w_0' : Reference load, N/m
W_0' : Dimensionless reference load, $W_0' = w_0'/E'R_0^2$
x : Coordinate, m
X : Dimensionless coordinate, $X = x/b$
z : Coordinate, m
Z : Dimensionless coordinate, $Z = z/h$
Z_1 : Viscosity-Pressure index
θ : Dimensionless film temperature, $\theta = T/T_0$
θ_1 : Dimensionless pinion teeth surface temperature, $\theta_1 = T_1/T_0$
θ_2 : Dimensionless gear teeth surface temperature, $\theta_2 = T_2/T_0$
μ : Equivalent viscosity, Pa · s
$\bar{\mu}$: Dimensionless equivalent viscosity, $\bar{\mu} = \mu/\mu_0$
μ_0 : Inlet viscosity, Pa · s
τ : Shear stress of lubricant, Pa
ρ : Density of lubricant, kg/m^3
ρ_0 : Inlet density of lubricant, kg/m^3
ρ_p : Inlet density of lubricant ,kg/m^3
$\bar{\rho}$: Dimensionless density of lubricant, $\bar{\rho} = \rho/\rho_0$
λ : Concentration by weight of Solid Lubricant
$\bar{\varphi}$: Pressure Angle, degree

2. Load, curvature and velocity

It is difficult to estimate the transmitted force between two teeth in a meshing gear. In this analysis, gear tooth load is assumed to act along the line of action. The gear teeth are assumed to be rigid and the dynamics of the gear are neglected. The pitch error is assumed

to be very small and will not influence the load. With these assumptions the load will be constant as long as two pairs of gear teeth carry the total load. When only one pair carries the load, the gear tooth load will immediately be doubled.

The contact between gear teeth at a distance $\bar{S}$ from the pitch line in a pair of involute gear teeth having radii r_a and r_b and a pressure angle $\bar{\psi}$ can be represented by two circular cylinders rotating with the same angular velocity ω_a and ω_b as the gear teeth themselves. These radii vary along the line of the action as:

$$R_1(\bar{S}) = r_a \sin(\bar{\psi}) - \bar{S} \quad (1)$$

$$R_2(\bar{S}) = r_b \sin(\bar{\psi}) + \bar{S} \quad (2)$$

The teeth both roll and slide against each other except at the pitch point, where a pure rolling condition exists. The tooth surface velocities are:

$$u_1(\bar{S}) = \omega_a R_1(\bar{S}) \quad (3)$$

$$u_2(\bar{S}) = \omega_b R_2(\bar{S}) \quad (4)$$

3. Governing Equations

In this study, for low particle concentration in the liquid-solid lubricant, single-phase flow can be assumed as a simplication. The time-dependent thermo-elastohydrodynamic lubrication of rolling/sliding line contacts can be solved simultaneously by using the modified Reynolds, elasticity, and energy equations to obtain pressure, film temperature, film thickness, friction coefficient and powder load carrying.

3.1 Modified Reynolds Equation

The relationship between shear stress and shear rate of non-Newtonian lubricant in this work can be approximated using a power-law viscosity model.

$$\tau_{xz} = \mu^* \frac{\partial u}{\partial z} \qquad and \qquad \tau_{yz} = \mu^* \frac{\partial v}{\partial z}$$

Where the equivalent viscosity

$$\mu^* = m_0 \left[\left(\frac{\partial u}{\partial z} \right)^2 + \left(\frac{\partial v}{\partial z} \right)^2 \right]^{(n-1)/2}$$

The dimensionless modified Reynolds equation for the transient thermal line contact problem with consideration of the temperature dependency of viscosity and density across the film [10] has been formulated using perturbation technique.

$$\frac{\partial}{\partial X}\left(\Phi \frac{\partial P}{\partial X} \right) = \Lambda \left\{ C_{UT}(\bar{t}) \frac{\partial}{\partial X}(\bar{\rho} H) + \frac{\partial}{\partial \bar{t}}(\bar{\rho} H) \right\} \quad (5)$$

Where

$$\Phi = \frac{\bar{\rho} H^3}{\bar{\mu}_U^*}, \Lambda = \frac{12 u_0 \mu_0 R_0^2}{b^3 P_H}, \bar{\mu}_U^* = \bar{\mu}_R n K_{SH} (\bar{I}^*)^{(n-1)/2} \text{ and } K_{SH} = \frac{m_0}{\mu_0} \left(\frac{u_0 R_0}{b^2} \right)^{(n-1)/2}$$

The boundary conditions are

$$X = X_{inlet}, P = 0 \quad ; \quad X = X_{exit}, P = \partial P / \partial X = 0$$

3.2 The apparent viscosity equation

The apparent viscosity in the power-law model needs to be included as a correction factor for viscosity temperature-pressure and the correction factor for solid particles in the lubricants according to Rylander[16] and Roelands[17]. The dimensionless apparent viscosity can be written as

$$\mu = \mu_0 \bar{\mu}_P \bar{\mu}_R \bar{\mu}_S^* \quad (6)$$

where

Journal of Template

Vol. 00, No. 0, 0000

$$\bar{\mu}_P = 1 + \frac{2.5\lambda\rho_0}{\lambda\rho_0 + (1-\lambda)\rho_p}$$

$$\bar{\mu}_R = \exp\{(\ln(\mu_0) + 9.67)(-1 + (1 + 5.1\times10^{-9}P_H P)^{z_1}) - \gamma T_0(\theta - 1)\}$$

$$\bar{\mu}_S^* = K_{SH}(\bar{I}^*)^{(n-1)/2}$$

3.3 The density equation

The density of the liquid-solid lubricant according to Dowson and Higginson[1] obeys the following relation

$$\rho = \frac{\rho_0 \bar{\rho}_D}{\bar{\rho}_P} \tag{7}$$

where

$$\bar{\rho}_P = 1 - \lambda\left(1 - \frac{\rho_0}{\rho_p}\right), \qquad \bar{\rho}_D = \left(1 + \frac{0.6\times10^{-9}P_H P}{1 + 1.7\times10^{-9}P_H P}\right)\left(1 - \beta T_0(\theta - 1)\right)$$

3.4 Thermal conductivity of oil film

The effect of pressure on thermal conductivity has been implemented in the thermal EHD calculation by Wang.[18]

$$\bar{k}_P = 1 + \frac{\alpha_{K,1}P_H P}{1 + \alpha_{K,2}P_H P} \tag{8}$$

3.5 The film thickness equation

The film thickness, including the deformation of surface under line contact, is given as

$$H = H_0 + \frac{X^2}{2C_{RT}} + D(X) - \frac{1}{\pi}\int_{X_{inlet}}^{X_{exit}} P(X')\ln|X - X'|dX' \tag{9}$$

where $D(X)$ is the dimensionless combined surface roughness of gear and pinion with random roughness distribution.

3.6 Load carrying capacity

The total load carrying capacity of the liquid-solid lubricant film consists of two parts: the first load component results from deformation of particles w_p, and the other load component is due to hydrodynamic action w_f, where

$$w_f = \int_{x_{inlet}}^{x_{exit}} p(x)dx \tag{10}$$

Consider a spherically shaped particle in the contact region under the action of normal load, the particle may undergo plastic deformation. For a particle that deforms plastically when the mean contact pressure reaches the hardness of particle,H_d , the load carrying capacity by a plastically deformed was written by Hua and Khonsari[19]

$$w_{i,pl} = \frac{9}{6}\pi^3 H_d^3\left(\frac{d_p}{E_{ps}}\right) + p(x)v_p A_{i,pl}$$

where

$$\frac{1}{E_{ps}} = \frac{1}{2}\left(\frac{1 - v_p^2}{E_p} + \frac{1 - v_s^2}{E_s}\right)$$

Where $A_{i,pl}$is the contact area of an individual particle due to plastic deformation. Equations give the load carrying capacity of a single particle due to plastic deformation. Therefore, the load carrying capacity for all particles is

$$w_p = \sum_{1}^{N_X}\sum_{1}^{N_Z} w_i \tag{11}$$

where N_X and N_Z are numbers of particles that come in contact with the surface in x-directions and z-directions respectively. The number of particles can be calculated as [8]:

$$N_j = l_j \sqrt{\frac{V_f}{l_X l_Z} \frac{6\lambda}{\pi d_p^3} \frac{\rho_0/\rho_p}{\left[1-\lambda\left(1-\rho_0/\rho_p\right)\right]}}$$

where λ is the concentration of particles by weight, V_f is the volume of the solid-liquid lubricant within the contact region and l_j is the effective length along which the particles deform. For line contact configuration where $l_Z = 1$, the total load carried by the solid-liquid lubricant can be expressed as

$$w_T = w_f + w_p$$

3.7 The load equation

The total load carrying capacity of the lubricant is due to hydrodynamic action. The dimensionless form of load balance equation is

$$\int_{X_{inlet}}^{X_{exit}} P dX = C_{WT}\left(\frac{W_T - W_P}{W_T}\right)\left(\frac{\pi}{2}\right) \tag{12}$$

3.8 The friction coefficient

The friction coefficient on pinion tooth surface is defined as

$$f = \frac{\mu_0 u_0 R_0}{w_0' b C_{WT}} \int_{X_{inlet}}^{X_{exit}} \left(\frac{\bar{\mu}^*}{H}\right)\left(\frac{\partial u^*}{\partial Z}\right)_{Z=0} dX + \frac{f_p E' R_0 W_p}{w_0' C_{WT}} \tag{13}$$

3.9 Energy equation

The surface in the contact region can be simplified as a semi-infinite body. Following Carslaw and Jaeger[19], the heat conduction in the surface can be analyzed by ignoring the heat conduction in the X and Ydirections. The time-dependent dimensionless energy equation for the oil film can be written as

$$\frac{\partial^2 \theta}{\partial Z^2} = K_{T1}\frac{\bar{\rho} H^2}{\bar{k}_p}\left(\frac{\partial \theta}{\partial \bar{t}} + u^*\frac{\partial \theta}{\partial X}\right) - K_{T2}\frac{\bar{\mu}}{\bar{k}_p}\left(\frac{\partial u^*}{\partial X}\right)^2 - K_{T3}\frac{\theta H^2}{\bar{k}_p}\left(\frac{\partial P}{\partial \bar{t}} + u^*\frac{\partial P}{\partial X}\right)$$

$$- K_{T4}|S_0 C_{UT}|\frac{H^2 f_p W_P}{\bar{k}_P \bar{A}_h} \tag{14}$$

where

$$K_{T1} = \frac{u_0 \rho_0 c_P b^3}{k_0 R_0^2}, \quad K_{T2} = \frac{\mu_0 u_0^2}{k_0 T_0}, \quad K_{T3} = \frac{\beta u_0 b^3 P_H}{k_0 R_0^2}, \quad K_{T4} = \frac{2 u_0 E' b}{k_0 T_0}$$

The boundary conditions of the energy equation[20] are

$$\theta(X_{inlet}) = 1$$

$$\theta_{1/2} = 1 \pm \frac{k_0 R_0}{\sqrt{\pi \rho_{1/2} c_{P,1/2} k_{1/2} b^3 u_0 C_{UT}\left(1 - \frac{S_0}{2}\right)}} \int_{X_{inlet}}^{X_{exit}} \left(\frac{\bar{k}_P}{H}\right)\left(\frac{\partial \theta}{\partial Z}\right)_{Z=0/1} \frac{dX'}{\sqrt{X - X'}}$$

4. Computational procedure and numerical method

The numerical solution of the governing equations described above is carried out by the pressure-temperature iteration between transient Reynolds, elasticity, powder load carrying capacity and energy equations for the thermo-elastohydrodynamic lubrication with liquid-solid non-Newtonian lubricants solutions were calculated using multigrid with full approximation scheme technique to improve the convergence rate. The convergence criteria of pressure, temperature, and hydrodynamic load are adopted as follows:

$$\sum_{i=0}^{N}\left|P_i^{k+1}-P_i^k\right| \Big/ \sum_{i=0}^{N} P_i^{k+1} \le 0.0001 \tag{15}$$

$$\sum_{i=0}^{N}\left|\theta_i^{k+1}-\theta_i^k\right| \Big/ \sum_{i=0}^{N} \theta_i^{k+1} \le 0.0001 \tag{16}$$

$$\left|C_{WT}\left(\frac{\pi}{2}\right)-\int_{X_{inlet}}^{X_{exit}} P dX\right| \Big/ C_{WT}\left(\frac{\pi}{2}\right) \le 0.0001 \tag{17}$$

During each time interval, the modified Reynolds equation, elasticity equation and energy equation are calculated using boundary conditions and initial conditions to obtain pressure and temperature distributions. In this problem, the boundary conditions X_{inlet} and X_{exit} can be obtained as$X_{inlet} = -6.0$ and $X_{exit} = +2.0$.

5. Results and Discussion

The gear data and the properties of liquid lubricant, solid particle and gearbox data used in the analysis are given in Table 1 and Table 2. These gear data correspond to a commercially available gearbox.

Table 1 Gear data and lubricant properties

Gear Material	UNB C61300
Number of teeth (pinion : gear)	35:140
Module, mm	2
Contact ratio	1.786
Pinion speed, rpm	1,000
Nominal pressure angle, degree	20
Teeth width, mm	20
Transmitted power, kW	10.0
Elastic modulus of pinion and gear, GPa	117.0
Density of the teeth of pinion and gear, kg/m^3	7950.0
Poisson ratio of the teeth of pinion and gear	0.28
Specific heat of the teeth of pinion and gear, J/kg · K	736.8
Combined surface roughness amplitude (R_{rms}), μm	0.10
Inlet temperature of lubricant, K	313.15
Ambient density of the lubricant, kg/m^3	892.80
Ambient viscosity of the lubricant, Pa · s	0.195
Viscosity-Pressure index(Z_1)	0.5685
Viscosity-Temperature coefficient, K^{-1}	0.05763
Coefficient of thermal expansivity, K^{-1}	0.00074
Thermal conductivity of lubricant, W/m · K	0.126
Specific heat of lubricant, J/kg · K	1870
Power law index (n) - liquid-solid lubricant	1.00969
- liquid lubricant	1.000

Fig. 1 shows the variation of the dimensionless idealized load, central pressure, dimensionless equivalent curvature and entrainment velocity along the line of action. The dimensionless load (C_{WT}.) is 0.5 at the approach point A and suddenly increased to 1.0 at point B ($\bar{S} = -1.10$ mm) when the load was carried by one pair of teeth beginning at that moment. The next pair of teeth comes into action at point D ($\bar{S} = 0.90$ mm) and the load is suddenly decreased to 0.5 again. The amount of sliding reaches its highest level at the

approach point. There is no sliding at the pitch point. The slip ratio reaches its highest level at the approach point. The entrainment velocity and the equivalent curvature have their lowest levels at approach point (point A) too. That means approach point might be the most critical from a lubricant film thickness point of view.

Table 2 Physical properties of solid lubricant particles

Solid particle properties	MoS_2
Brinell hardness, GPa	3.139
Modulus of elasticity, GPa	34
Poisson ratio	0.13
Density, kg/m^3	4800
Friction coefficient	0.1
Particle diameter, μm	2

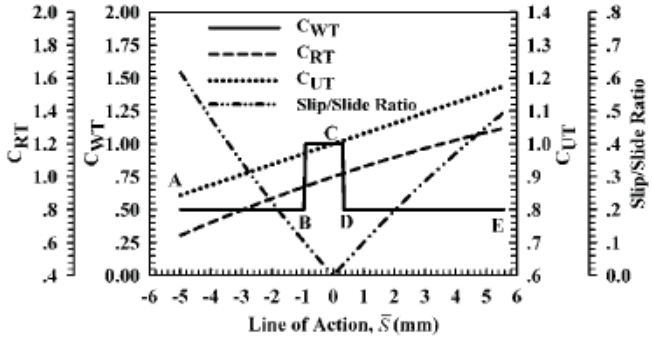

Fig.1 Variation of the load, central pressure, equivalent curvature and entrainment velocity along the line of action.

Fig. 2 shows the variation of minimum film thickness along the line of action of the gear tooth for liquid lubricant (SAE 90) and liquid-solid lubricant (SAE 90 plus 10% MoS_2 by weight) and the amplitude of combined roughness(R_{RMS}) is 0.10 μm,. It can be seen that the minimum film thickness of liquid-solid lubricant is higher than the minimum film thickness for liquid lubricant along the line of action because of the load carried by the solid particles in lubricant. At the approach point($\bar{S} = -4.97$ mm), the film thickness is at its lowest value; the minimum film are 0.17 μm for all lubricants. This behavior can be understood by the mechanism of the squeeze effect.

The transient effect is most pronounced after points B and D. When the load is suddenly increased at point B($\bar{S} = -0.90$ mm), the minimum film thickness first increases from 0.84 μm to 0.86 μm for the liquid lubricant, and from 0.97 μm to 0.99 μm for liquid-solid lubricant; then it decreases to 0.76 μm for the liquid lubricant, and to 0.90 μm for liquid-solid lubricant, before it increases again. It never reaches an equilibrium state until the load is halved again. When the next pair of teeth comes into action at point D ($\bar{S} = 0.40$ mm), the load is suddenly decreased. The minimum film thickness first increases from 0.92 μm to 1.04 μm for the liquid lubricant and 1.05 μm to 1.19 μm for liquid-solid lubricant; then it decreases until it recovers at 1.20 mm approximately, where the minimum film thickness values are 0.83 μm and 0.99 μm for liquid lubricant and liquid-solid lubricant, respectively. It approaches the steady state condition at approximately 3.53 mm.

Journal of Template

Vol. 00, No. 0, 0000

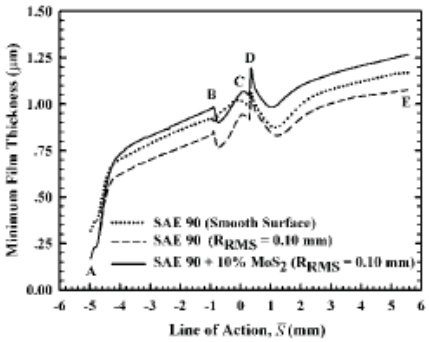

Fig. 2 Variation of minimum film thickness along the line of action for liquid lubricant and liquid-solid lubricant

The variation of friction coefficient on pinion tooth and temperature rise of oil film for liquid lubricant and liquid-solid lubricant, for rough surface gear teeth along the line of action are presented in Fig. 3 and Fig. 4. The friction coefficient and temperature rise of oil film for the liquid-solid lubricant are lower along the line of action than those for liquid lubricant except the near pitch point, where they are higher value. At the approach point (point A, $\bar{S} = -4.97$ mm), the friction coefficient and maximum film temperature are 0.164 and 107.71 ^{o}C, respectively, for liquid lubricant and 0.158 and 107.37 ^{o}C, respectively, for liquid-solid lubricant when contact moves along the line of action. The first peak value is at -4.83 mm for the friction coefficient and at -4.63 mm for the maximum film temperature, where the friction coefficient and the maximum film temperature are 0.219 and 238.07 ^{o}C for liquid lubricant and 0.203 and 217.47 ^{o}C for the liquid-solid lubricant, respectively then decreases until the load is suddenly increased. At $\bar{S} = -0.40$ mm, the friction coefficient and maximum film temperature are 0.561, 254.25 ^{o}C, for liquid lubricant and0.451 and 250.37 ^{o}C, for the liquid-solid lubricant respectively. The values then decrease to the minimum value at the pitch point. At the pitch point (point C), the friction coefficient and maximum film temperature for liquid-solid lubricant have a higher value than the value for liquid lubricant, because of friction forces and friction heating of solid particle, These values are 0.077, 61.73 ^{o}C, 0.079 and 63.08 ^{o}C for liquid lubricant and liquid-solid lubricant, respectively. The friction coefficient is approximately zero and the maximum temperature is near the ambient temperature because there is no sliding. Adjacent to the approach point the friction coefficient and maximum temperature rise all have high levels because of the high load even though the contact surface is small. The highest temperature rise occurs at the approach point, which is caused by the large slip ratio. When the line of action shifts from the pitch point, film temperature and friction coefficient rise up again. At $\bar{S} = +0.30$ mm, the maximum values are 0.342 and 115.85 ^{o}C for liquid lubricant, and 0.285 and 105.72 ^{o}C for liquid-solid lubricant. When the next pair of teeth comes into action at point D, the film temperature and friction coefficient suddenly decrease and then increase again when contact moves along the line of action. One can see that the maximum temperature rise at the approach point is higher than at the recess point. That is because the slip ratios of the approach point are larger than those of the recess point.

Journal of Template

Vol. 00, No. 0, 0000

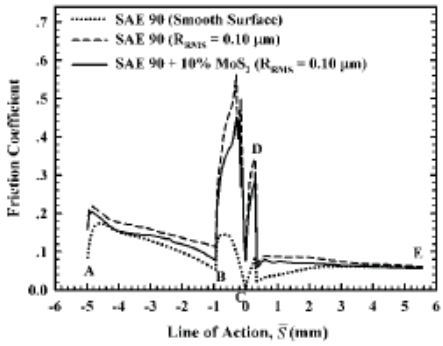

Fig. 3 Variation of friction coefficient on pinion surface along the line of action for liquid lubricant and liquid-solid lubricant

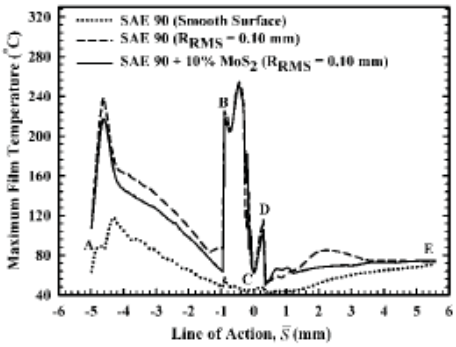

Fig. 4 Variation of maximum temperature rise along the line of action for liquid lubricant and liquid-solid lubricant

Fig. 5 and Fig. 6 show the minimum film thickness, friction coefficient and maximum film temperature at the approach point A, point B where the load is suddenly increased to double and at pitch point C as a function of amplitude of combined surface roughness for a liquid-solid lubricant. The results show that the amplitude of combined surface roughness has a significant effect on film temperature and friction coefficient in liquid-solid TEHL of spur gears. Minimum film thickness decreases but friction coefficient and maximum film temperature increase when amplitude of combined surface roughness increases. At approach point (point A), minimum film thickness, friction coefficient and maximum film temperature are 0.32 μm, 0.075 and 59.73 °C, respectively for smooth surface and they are 0.17 μm, 0.158, 107.37 °C and 0.14 μm, 0.183 and 128.81 °Cwhen amplitudes of combined surface roughness are 0.10 μm and 0.12 μm, respectively. At the point the load is suddenly increased (point B), minimum film thickness, friction coefficient and maximum film temperature are 1.02 μm, 0.118 and 59.09 °C for smooth surface, and they are 0.98 μm, 0.220, 218.27 °C, 0.97 μm, 0.233 and 254.75 °C when amplitudes of combined surface roughness are 0.10 μm and 0.12 μm, respectively. At the pitch point (point C), minimum film thickness, friction coefficient and maximum film temperature are 1.16 μm, 0.008 and 45.41 °C for smooth surface and they are 1.06 μm, 0.079, 63.08 °C, 1.03 μm, 0.089 and 67.35 °C when amplitudes of combined surface roughness are 0.10 μm and 0.12μm, respectively.

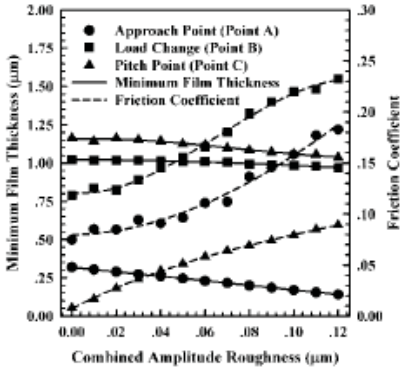

Fig. 5 Variation of minimum film thickness and friction coefficient with amplitude combined surface roughness for liquid-solid lubricant

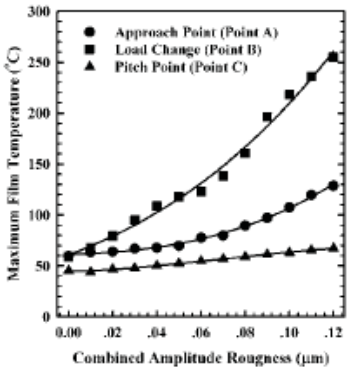

Fig. 6 Variation of maximum temperature rise with amplitude of combined surface roughness for liquid-solid lubricant

The variation of friction coefficient on pinion tooth, minimum film thickness and temperature rise of oil film for liquid-solid lubricant gear teeth along the line of action are presented in Fig. 7 and Fig. 8. The minimum film thickness, friction coefficient and maximum film temperature at the approach point (point A) are only insignificantly effect by roughness for liquid-solid TEHL in spur gears. At the point with suddenly increased load (point B), the minimum film thickness increases when concentration of solid particles increases. It is 0.86 μm for liquid lubricant and it increases to 0.99 μm and 1.05 μm when concentrations of solid particle are 10% and 20% by weight, respectively. The friction coefficient and maximum film temperature decreased when concentration of solid particle decreases. They are 0.254 and 224.90 °C for the friction coefficient and maximum film temperature, respectively, when lubricant is purely liquid lubricant, and they decrease to 0.220 and 218.27 °C when the concentration of solid particles is 10% by weight. When concentration of solid particles is 20% by weight, friction coefficient and maximum film temperature are 0.194 and 205.48 °C, respectively. The friction coefficient and maximum film temperature values for liquid-solid lubricant are lower than the values for liquid lubricant when load is suddenly increased (point B), because the effect of particle load carrying would be to decrease the load of the liquid film lubricant. At the pitch point (point C), the minimum film thickness, friction coefficient and maximum film temperature

for liquid-solid TEHL in spur gears increases when concentration of solid particles increases because there is no sliding.

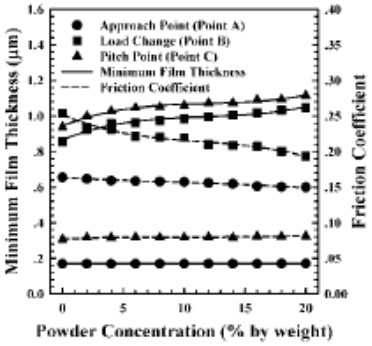

Fig. 7 Variation of minimum film thickness and friction coefficient on pinion surface with powder concentration for liquid-solid lubricant

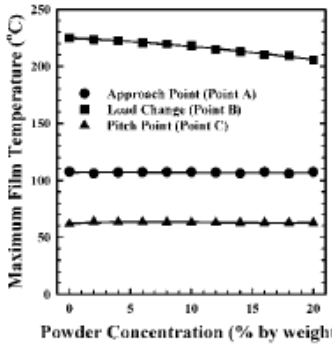

Fig. 8 Variation of maximum temperature rise with powder concentration for liquid-solid lubricant

In this paper, the approach point is where the gear teeth are in the first contact and at that point the film thickness has its lowest values; that means approach point might be the most critical from a lubricant film thickness point of view. The load of gear teeth may be increased more than the normal operating condition due to a sudden overload or impact of gear teeth. The characteristics of spur gears were investigated when subjected to a sudden overload of 25% of the normal operating load with liquid lubricant and liquid-solid lubricant as shown in Fig 9.

During sudden overload or impact load at the approach point (point I) when amplitudes of combined surface roughness are 0.10 μm, the minimum film thickness for liquid lubricant and liquid-solid lubricant is close to the normal operating conditions because at the approach point the minimum film thickness depends on the mechanism of the squeeze effect; the minimum film thicknesses at the approach point are 0.169 μm, 0.167 μm and 0.168 μm for normal operating conditions, sudden overload with liquid lubricant and sudden overload with liquid-solid lubricant, respectively. The friction coefficients and maximum film temperatures with sudden overload at the approach point are greater than the normal operating condition; they are 0.164 and 107.71 °C, 0.200 and 124.84 °C and 0.172 and 119.18 °C for normal operating condition and sudden

overload at the approach point operating condition with liquid-solid lubricant, respectively. When the contact moves forward along the line of action, the minimum film thickness, friction coefficient and maximum film temperature rapidly increase. At point J, the minimum film thickness, friction coefficient and maximum film temperature for normal operating condition with liquid lubricant, sudden overload operating condition with liquid lubricant and sudden overload operating condition with liquid-solid lubricant are 0.586 μm, 0.184 and 174.30 °C, 0.522 μm, 0.213 and 215.32 °C and 0.621 μm, 0.195 and 200.31 °C, respectively. When the load is suddenly decreased at point K, the minimum film thickness for impact overload operating condition are rapidly increased to 0.654 μm and 0.773 μm for liquid lubricant and liquid-solid lubricant, respectively but the friction coefficient and maximum film temperature are rapidly decreased to 0.175 and 158.61 °C and 0.157 and 141.79 °C as shown in Fig 10, Fig. 11 and Fig. 12.

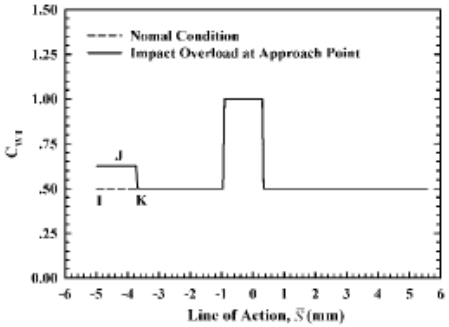

Fig. 9 Variation of the load, along the line of action for sudden overload at approach point

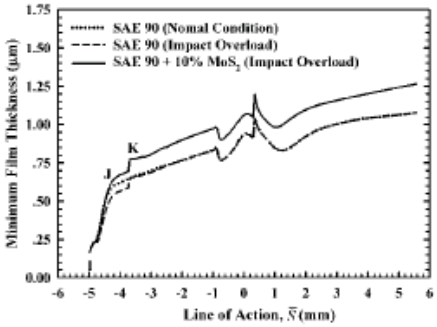

Fig. 10 Variation of minimum film thickness along the line of action for sudden overload at approach point with liquid lubricant and liquid-solid lubricant

In the impact load region, the minimum film thickness for liquid-solid lubrication is greater than the minimum film thickness for liquid lubrication but the friction coefficients and maximum film temperatures for liquid-solid lubricant are smaller than the friction coefficients and maximum film temperatures for liquid lubricant because of the load carried by solid particle in the lubricant and the change of lubricant properties from Newtonian fluid for liquid lubricant to dilatant fluid when solid particles are added into the lubricant.

Fig. 13 and Fig. 14 shown the variation of friction coefficient on pinion tooth, minimum film thickness and temperature rise of oil film for liquid-solid lubricant gear teeth along the line of action with impact overload at the approach point. At the approach point (point I), the concentration of solid particle has an insignificant effect on the minimum film

thickness and maximum film temperature, but the friction coefficient first decreases until concentration of solid particle is more than 10% by weight, then it increases again. When the contact moves forward along the line of action to point J and Point K, the minimum film thickness increases but the friction coefficient and maximum film temperature decrease when concentration of solid particle increases. This is because the effect of particle load carrying would be to decrease the load of the liquid film lubricant.

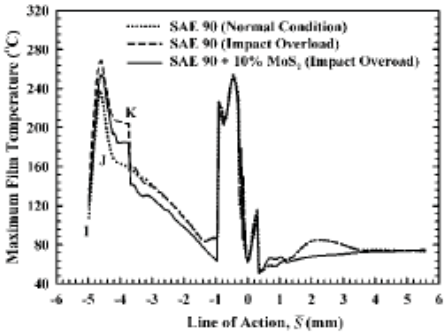

Fig. 11 Variation of maximum film temperature along the line of action when sudden overload at approach point with liquid lubricant and liquid-solid lubricant

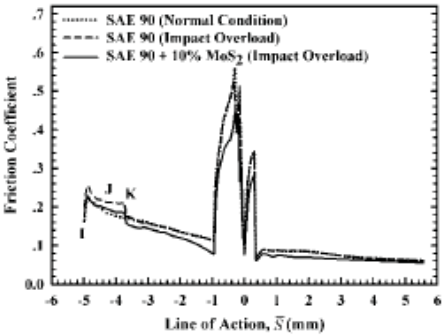

Fig. 12 Variation of friction coefficient along the line of action under sudden overload at approach point with liquid lubricant and liquid-solid lubricant

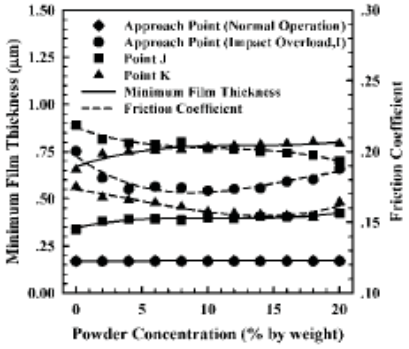

Fig. 13 Variation of minimum film thickness and friction coefficient with powder concentration under sudden overload at approach point for liquid-solid lubricant

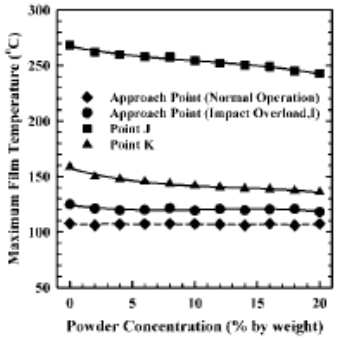

Fig. 14 Variation of maximum temperature rise with powder concentration under sudden overload at approach point for liquid-solid lubricant

6. Conclusion

The time dependent modified Reynolds equation, energy equation and powder load carrying were formulated for spur gear with liquid-solid lubricant to obtain minimum film thickness, maximum film pressure, friction coefficient and maximum film temperature in the contact between two rough gear teeth of involute spur gears. The dynamic characteristics of spur gears under TEHL were investigated for both liquid and liquid-solid lubricants. The load is kept constant as long as two pair of teeth carried the total load and it is doubled when only one pair is in action. The following can be concluded as:

1. Minimum film thickness of liquid-solid lubricant is higher than the minimum film thickness of liquid lubricant along the line of action, but friction coefficient and maximum film temperature are lower value than that the liquid lubricant except the pitch point where they are higher value.

2. Considering the rough surface effect, the minimum film thickness is thinner but the maximum film temperature and friction coefficient are greater when the amplitude of combined surface roughness increases. Therefore, the surface roughness of gear teeth significantly affects tribology of gear teeth and should be considered in gear design application.

3. When concentration of solid particle increases, the minimum film thickness increases but friction coefficient and maximum film temperature decrease. The sizes of solid particles in liquid-solid lubricant have an insignificant effect for rough liquid-solid TEHL in spur gear.

4. For spur gears with liquid-solid lubricant under sudden overload at the approach point, the film temperature and friction coefficient are decreases but minimum film thickness increase when compared with liquid lubricant that means liquid-solid lubricant can be protect the damage of gear teeth under severe operating condition.

7. References

(1) Dowson D., Higginson G. R., *Elastohydrodynamic lubrication, the fundamentals of roller and gear lubrication.*, Oxford: Pergamon; 1966.

(2) Wang KL, Cheng H. S., *A numerical solution to the dynamic load, film thickness and surface temperatures in spur gears, Part I - analysis.*, ASME J Mech Design 1981, Vol. 103, pp. 177–87.

(3) Wang KL, Cheng H. S., *A numerical solution to the dynamic load, film thickness and surface temperatures in spur gears, Part II - results.*, ASME J Mech Design 1981Vol. 103, pp. 188–94.

(4) Hua D. Y. and Khonsari M. M., *Application of transient elastohydrodynamic lubrication analysis for gear transmissions.*, STLE Tribol Trans 1995, Vol.38, pp. 905–13.

(5) Larsson R., *Transient non-Newtonian analysis of an involute spur gear.*, Wear, 1997, Vol. 207, pp. 67–73.

(6) Wang Y., Li H., Tong J. and Yang P., *Transient thermoelastohydrodynamic lubrication analysis of an involute spur gear*, Tribology International, 2004, Vol. 37, pp. 773–782.

(7) Mongkolwongrojn M. and Panichakorn J., *TEHL Analysis of Rough Surface Spur Gears with Non-Newtonian Lubricants Under Sudden Overloads*, JSME Journal of Advanced Mechanical Design, Systems, and Manufacturing, 2012, Vol.6 No.7, pp. 1031-1045.

(8) Sayles R.S. and Ioannides E., *Debris damage in rolling bearings and its effects on fatigue life*, ASME J Tribol, 1988, Vol. 110, pp. 26–31.

(9) Khonsari M.M., Wang H. S., and Qi Y.L., *A Theory of Liquid-Solid Lubrication in Elastohydrodynamic Regime*, ASME J. Tribol., 1989, Vol. 111, pp. 256–265.

(10) A.E.Yousif and S.M.Nacy, *The lubrication of conical journal bearings with bi-phase (liquid–solid) lubricants*, Wear, 1994, Vol. 172, pp. 23–8.

(11) Mongkolwongrojn M., Aiumpornsin C. and Thammakosol K., *Theoretical Investigation in Thermoelastohydrodynamic Lubrication With Non-Newtonian Lubricants Under Sudden Load Change*, Journal of Tribol, 2006, Vol.128, pp.771–777.

(12) Lubrecht, A. A., Ten Napel, W. E., and Bosma, R., *Multi-grid, an Alternative Method for Calculating Film Thickness and Pressure Profiles in EHL Line Contacts*, ASME J. Tribol., 1986,Vol. 108, pp. 551–556.

(13) Osborn F.K. and Sadeghi F., *Time Dependent Line EHD Lubrication Using the Multigrid/Multilevel Technique*, ASME J. Tribology, 1992, Vol. 114, pp. 68–74.

(14) Ai X. and Cheng, S. H., *Transient EHL Analysis for Line Contacts With Measured Surface Roughness Using Multigrid Technique*, ASME J. Tribol. , 1994, Vol. 116, pp. 549–558.

(15) Wang W.Z., Chen H., Hu Y.Z. and Wang H., *Effect of surface roughness parameters on mixed lubrication characteristics*, Tribology International, 2006, Vol. 39, pp 522–527.

(16) RylanderH.G.,*A Theory of Liquid-Solid Hydrodynamic Film Lubrication*, ASLE Journal of the American Society of Lubrication Engineerings, 1966, pp.264-271.

(17) Roelands C. J. A., *Correlation aspects of viscosity-temperature-pressure relationship of lubricating oils.*, Ph.D. thesis, Delft Univeristy of Technology, Netherlands, 1966.

(18) Wang, S., Cusano C. and Conry, T. F., *Thermal analysis of elastohydrodynamic lubrication of line contact using the Ree-Eyring fluid model*, Journal of Tribology, 1991, Vol. 113, pp. 232-244.

(19) Hua, D. Y., and Khonsari, M. M., 1996, *Elastohydrodynamic Lubrication by Powder Slurries*, ASME J. Tribol., 118, pp. 67–73.

(20) Carslaw, J. W., and Jaeger, J. C., *Conduction of Heat in Solids*, Oxford University Press, 1959, London.

Western Digital (Thailand) Company Limited.
140 Moo2, Bangpa-In industrial Estate,
Udomsorayuth Road, Klongjig, Bangpa-In,
Ayutthaya 13160 Thailand.
Tel : 6635-277-000 Fax : 6635-277-111

วันที่ 3 สิงหาคม 2553

เรื่อง ขอเชิญอาจารย์เป็นวิทยากรบรรยายพิเศษ

เรียน คณบดี วิทยาลัยร่วมด้านเทคโนโลยีการบันทึกข้อมูลและการประยุกต์ใช้งาน

สถาบันเทคโนโลยีพระจอมเกล้าเจ้าคุณทหารลาดกระบัง

ด้วยทางบริษัท เวสเทิร์นดิจิตอล(ประเทศไทย) จำกัด ได้จัดตั้งสถาบัน ฝึกอบรม โดยได้รับการสนับสนุนจาก ศูนย์เทคโนโลยีอิเล็กทรอนิกส์และคอมพิวเตอร์ แห่งชาติ สำนักงานพัฒนาวิทยาศาสตร์และเทคโนโลยีแห่งชาติ เพื่อฝึกอบรม นักวิทยาศาสตร์และวิศวกร รวมถึงช่างเทคนิคของบริษัทฯ ตลอดจนวิศวกรของ ผู้ผลิตชิ้นส่วนในอุตสาหกรรมฮาร์ดดิสก์

บริษัทมีความเห็นว่า วิทยาลัยร่วมด้านเทคโนโลยีการบันทึกข้อมูลและการประยุกต์ใช้งาน สถาบันเทคโนโลยีพระจอมเกล้าเจ้าคุณทหารลาดกระบัง มีคณาจารย์ที่มีความรู้ความสามารถถ่ายทอดให้แก่ผู้เข้าอบรมได้

จึงใคร่ขอเรียนเชิญ รศ.ดร. มงคล มงคลวงศ์โรจน์ มาเป็นวิทยากรบรรยายดังต่อไปนี้

Tribology for Engineer (Thai Version) วันที่ 4 สิงหาคม 2553 เวลา 9.00 - 16.00 น.

จึงเรียนมาเพื่อโปรดพิจารณาอนุมัติ

(นายพรชัย จิตรนำทรัพย์)
ผู้จัดการอาวุโสฝ่ายพัฒนาทรัพยากรมนุษย์และโครงการวิจัย
บริษัท เวสเทิร์น ดิจิตอล (ประเทศไทย) จำกัด